ISET Journal of Earthquake Technology, Paper No. 556, Vol. 57, No. 3, September 2020, pp. 103-150

PROBABILISTIC SEISMIC HAZARD MAPPING OF NORTHWEST INDIA USING AREA SOURCES WITH NON-UNIFORM SPATIAL DISTRIBUTION OF SEISMICITY

A.K. Jaisal
Department of Civil Engineering, Indian Institute of Technology Kanpur
Kanpur 208016, E mail id: *akjaisal@gmail.com*

Ishwer D. Gupta
Row House 4, Suncity, Pune 411051
(formerly at CWPRS Pune and IIT Roorkee), E mail id: *idgrh4@gmail.com*

Vinay K. Gupta (Corresponding Author)
Department of Civil Engineering, Indian Institute of Technology Kanpur
Kanpur 208016, E mail id: *vinaykg@iitk.ac.in*

ABSTRACT

The northwest region of India is prone to very high level of seismic hazard due to the presence of the western Himalayan plate boundary within the region. To manage and mitigate the associated risk in an effective manner, it is necessary to have reliable and realistic mapping of seismic hazard in the region. This study presents a comprehensive seismic hazard analysis to prepare the probabilistic seismic hazard maps of northwest India in terms of 5%-damping spectral accelerations at different natural periods for rock-type site conditions in a significant updating of the results of the previous studies. Major improvements made in the present study include: use of non-uniform spatial distribution of the expected seismicity over each of the 16 area sources of shallow crustal earthquakes considered, consideration of the additional effect of deep focus earthquakes in Hindukush subduction zone by modeling this as a dipping plane source, selection of the most appropriate ground motion prediction equations (GMPEs) for both types of seismic sources by using the available strong motion data, and estimation of the source-to-site distance metrics consistent with the selected GMPEs. An empirical approach, based on a detailed seismic hazard analysis for different soil conditions, is also proposed to obtain realistic amplification factors for modifying uniform hazard response spectra for the rock sites to those for the soil sites with a given V_{S30} value. A critical comparison of the results of this study with those of the major past studies indicates large discrepancies and differences, which could be attributed to several unrealistic and subjective assumptions and idealizations made in the past studies. Finally, on comparing the present estimates with those prescribed by the Indian code IS 1893 (Part-1), it is found that one additional zone of greater hazard level may need to be introduced in the code. A simple modification involving the MCE-level hazard estimates for peak ground acceleration and 0.2-s spectral acceleration is also proposed in the Type-I spectral shape prescribed by the Indian code in order to raise the hazard levels for non-rigid structures.

KEYWORDS: Probabilistic Seismic Hazard; Northwest Himalayan Region of India; Seismic Sources; Ground Motion Prediction Equation (GMPE); Uniform Hazard Response Spectra; Site Amplification; Hindukush Subduction Zone

INTRODUCTION

The northwest India, being host to the highly seismic western Himalayan belt, is characterized by a very high level of seismic hazard. It is therefore vulnerable to significant risk levels due to the presence of some of the largest dams in the world like Bhakra and Tehri dams, several cities of high population density like Dehradun, Shimla, and Srinagar, and large inflow of tourists and pilgrims. The mitigation of this risk requires a reliable and realistic estimation of hazard based on a comprehensive database on past seismicity, seismotectonic features, and strong motion accelerograms, which would provide a sound basis for correctly anticipating the seismic response of structures and then coming up with appropriate strategies for the seismic design of new structures and seismic retrofitting of the existing structures. The

present study utilizes the probabilistic seismic hazard analysis (PSHA) approach to prepare macrozoning maps in terms of spectral acceleration (SA) amplitudes for the northwest Himalayan region of India, covering the states of Uttarakhand, Himachal Pradesh, and erstwhile Jammu & Kashmir (Union territories of Jammu and Kashmir, and Laddakh now). Many devastating earthquakes have occurred in the past in this region, and there is a significant potential for the occurrence of equally strong earthquakes in future. The most significant pre-instrumental earthquakes that affected the region are the 1505 Nepal earthquake and the 1803 Garhwal Himalayan earthquake, both with magnitudes above 8.0. The Kangra earthquake of 1905 with M_W = 7.8 has been termed as one of the four Great Indian earthquakes of the early instrumental period. The other damaging earthquakes of the instrumental period include the 1991 Uttarkashi (M_W = 6.9), 1999 Chamoli (M_W = 6.5), and 2005 Muzaffarabad (M_W = 7.6) earthquakes. In addition, the Hindukush subduction zone is characterized by several earthquakes with M_W > 7.5, which may contribute significantly to the long-period hazard in the region. As per the current Indian code of practice, IS 1893-1 (BIS [1]), the region has been classified into Zones IV & V, which are the zones with severe to very severe hazard.

The initial attempt on using the PSHA approach to prepare hazard map for the entire country was made by Basu and Nigam [2], in terms of PGA for the return period of 100 years. This was followed by the studies of Khattri et al. [3], and Bhatia et al. [4], who produced hazard maps for the country in terms of PGA for a return period of 475 years by characterizing the seismicity of the country with the help of broad seismic sources and by subjectively adopting a single ground motion prediction equation (GMPE) for the entire country. Parvez et al. [5] followed a deterministic approach to prepare a PGA-based hazard map for India by using synthetic ground motion data (Costa et al. [6]). The National Disaster Management Authority (NDMA), Government of India, also prepared hazard maps for the entire country in terms of PGA and SA at different natural periods for different return periods. This study used source-specific GMPEs developed based on the ground motion records simulated by the seismological source model approach (Boore [7]). Nath and Thingbaijam [8] produced the hazard maps by incorporating a logic tree framework in the PSHA approach. They considered eight GMPEs with equal weights for shallow crustal earthquakes in the Himalayas and four GMPEs with equal weights for the Hindukush subduction region. They also modelled the seismicity by assigning weights to the smooth-gridded (zoneless) and uniform seismicity models. Patil et al. [9] prepared PGA-based hazard maps for the 475-year and 2475-year return periods for the state of Himachal Pradesh and adjoining regions. They arbitrarily assumed the attenuation relation by Boore and Atkinson [10] and used the CRISIS software in their hazard computations. Rout et al. [11] also used the CRISIS software to compute hazard levels for the northwestern and central Himalayas and adjoining regions. They considered four published attenuation relations with equal weights in the logic tree approach to model the attenuation of ground motions.

This study carries out a comprehensive PSHA (Cornell [12, 13]; McGuire [14]) of the northwest Himalayan region of India by making use of the latest database available for the region in all the aspects of PSHA and by making scientifically rational assumptions for the aspects with insufficient data. Based on a critical analysis of the seismotectonic features and past seismicity of the region, a total of 16 area sources are identified to quantify seismic activity in the case of shallow crustal earthquakes along with one dipping-plane source of deep focus earthquakes in the Hindukush subduction zone. The cumulative form of the Gutenberg-Richter magnitude-frequency relation (Richter [15]) is fitted to the past earthquake data in each of these sources. The occurrence rates of different magnitudes of earthquake in a source are then obtained by defining an appropriate recurrence model with an upper bound magnitude for the source zone. The spatial distribution of seismicity within each source is carried out non-uniformly based on the past trends of seismic activity. For the source-to-site attenuation of ground motion, several recently published GMPEs for similar tectonic setups around the world are rigorously evaluated for their ability to replicate the ground motions recorded for the region under both shallow crustal and subduction zone earthquakes. Hazard maps are prepared in the form of contours for PGA and 5%-damping SA at four different periods in rock-site conditions for four different return periods. Finally, a hybrid approach based on the site amplification term in the selected GMPE for shallow crustal earthquakes is proposed to extend the so-obtained hazard results to softer soil conditions.

This study is characterized by several distinguishing features compared to the existing past studies for the region, thus resulting in significantly improved hazard estimation. This includes the use of a more comprehensive and thoroughly scrutinized earthquake catalogue, particularly for the pre- and early-instrumental periods, and a non-uniform spatial distribution of the estimated occurrence rates of earthquakes. Most other studies have used uniform distribution, which does not give a realistic spatial distribution of the hazard. Unlike any of the past studies, the GMPEs used are the best choices based on the available strong motion records among the GMPEs for shallow crustal and subduction zone earthquakes. Even for the area sources, the same type of source-to-site distances are estimated, as required in the selected GMPEs, by accounting for the effects of the rupture dimensions and the strike and dip angles. The hazard amplitudes and their spatial distributions in the hazard maps obtained in this study are able to depict the desired conformity with the observed trends of seismicity and the major tectonic features. These trends have been diluted strongly or lost completely in the past studies. This is demonstrated by comparing the DBE-level PGAs from the present study with those from the five other studies at 10 important cities spread over the study region. The presented hazard maps can thus be considered as an updating of the various existing maps.

SEISMOTECTONICS OF THE REGION

The region considered in this study is one of the most active orogenic regions in the world, the tectonic features of which are comprehensible within the framework of intercontinental drift theory. The collision of Indian and Eurasian plates about 40–50 million years ago resulted in the complete subduction of Tethys oceanic crust and emergence of the Himalayan ranges. The Indian plate is still moving in the north-northeast direction at a rate of about 5 cm/year (Molnar and Tapponnier [16]). A major part of this rate can be attributed to the crustal shortening of the upper Indian plate by the formation of a series of nappes, thrust faulting, and folding, which resulted in the formation of Himalayan ranges. Figure 1 shows major tectonic features in the north-west Himalayas and the adjoining regions bounded by the latitudes $25.0^{o}-40.0^{o}$ N and longitudes $69.5^{o}-84.0^{o}$ E. This is based on the Seismotectonic Atlas of India (GSI [17]) for the region within the Indian territory, and on the publications like Hodges [18], Taylor et al. [19], Singh et al. [20], PMD-NORSAR [21], Robinson [22], Taylor and Yin [23], and Lin et al. [24] for the region beyond the boundaries of India. The complete region of Figure 1 can be subdivided into six broad tectonic provinces, viz., the western Himalayas and western part of central Himalayas, Hindukush-Pamir ranges, Karakoram region, Trans-Himalayas and Tibetan plateau, Kirthar-Sulaiman ranges, and the Indo-Gangetic plain adjacent to the west and south of the Himalayan arc.

1. Western Himalayas and Western Part of Central Himalayas

The Himalayan arc defining the northern boundary of Indian tectonic plate extends for more than 2400 km from the Hazara-Kashmir Syntaxis in the west to the Namche Barwa Syntaxis in southeastern Tibet. The seismicity of the entire Himalayan belt can be associated with periodical stick-slip displacements along a sub-horizontal decollement interface of the main Himalayan thrust (MHT) fault. The MHT is a gently dipping plane separating the Indian and Eurasian plates at a depth of about 5 km near the main frontal thrust (MFT) in the south to about 20 km near the main central thrust (MCT) in the north (Seeber and Armbruster [25]). To the north of detachment, there exists the Indus Tsangpo suture zone (ITSZ), which separates the Indian continental plate from the Tibetan plate. The various fault planes, viz., the main central thrust (MCT) and main boundary thrust (MBT), merge with this detachment at steep angles. The ITSZ and the MCT, MBT, and MFT faults from north to south form four major fault systems along the entire length of the Himalayan arc. There are also a large number of faults running in the transverse and oblique directions, thus fragmenting the longitudinal faults into the lengths of about 100–150 km. The prominent transverse faults in the study region include Kishtwar, Sundernagar, Tankpur, Karnali, Samea, and Dhangsi faults, as shown in Figure 1.

The Himalayan arc can be considered to comprise the western, central, and eastern stretches, with somewhat varying geodynamic characteristics (Gupta [26]). The study region here includes about 1000 km length of the Himalayan arc, covering (a) about 600 km of western Himalayas from the western Syntaxis around the 73°E longitude up to the 80°E longitude near the western boundary of Nepal, and (b) about 400 km of the western part of the central Himalayas further east up to the 84°E longitude. The

western Himalayas can be segmented from west to east into six blocks, viz., Kashmir, Kishtwar, Kangra, Shimla, Garhwal, and Kumaon blocks, which are separated by prominent transverse tectonic or geological features. Thus, for the purpose of seismic hazard analysis, it is necessary that the Himalayan arc in the study region here is suitably divided into several source zones.

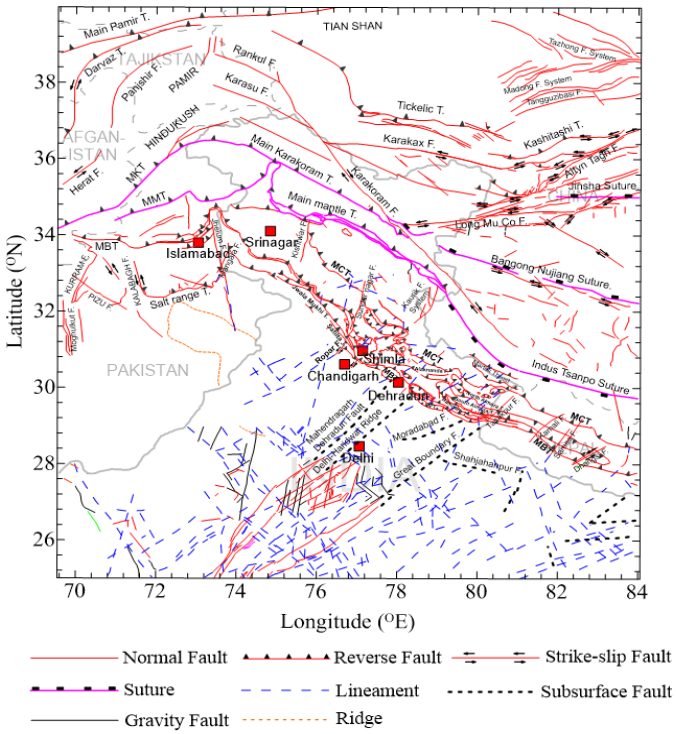

Fig. 1 Major tectonic features in north-west Himalayas and adjoining region

2. Hindukush-Pamir Ranges

The Hindukush-Pamir ranges lie in northern Afghanistan and are bounded in the west by the sinistral Darvaz and Chaman faults, in the east by the dextral Karakoram fault, and in the south by two sutures known as the main Karakoram thrust (MKT) and main mantle thrust (MMT). These ranges are characterized by a high concentration of intermediate-depth seismicity (i.e., within 70–300 km). This is also by far the most active region in the world, which is not associated with the subduction of oceanic lithosphere (Searle et al. [27]). The subducting northernmost leading edge of the Indian crust forms a Wadati-Benioff zone, dipping very steeply northward under the western and central parts of the Hindukush range and southward under the Pamirs trending NE-SW (Billington et al. [28]; Pegler and Das [29]). To further north in the Pamir mountain ranges, lie the main Pamir thrust fault and other faults, which are a source of frequent shallow crustal earthquakes.

3. Karakoram Region

The Karakoram region hosts two major thrusts, namely MMT and MKT, and Karakoram fault, which is a major dextral strike-slip fault extending for almost 1,000 km from central Pamir to Kumaon Himalayas.

4. Trans-Himalayas and Tibetan Plateau

The Trans-Himalayan and Tibetan plateau region is traversed by several sutures, including the Bangong-Nujiang and Jinsha sutures running in the east-west direction. The Tibetan region is also cut by a number of large sinistral strike-slip faults, like the Altyn Tagh and Kunlun faults, trending in the east-west direction. Karakax, the western portion of the Altyn Tagh fault, is the largest strike-slip fault on the northwestern Tibetan rim. This accommodates most of the eastward movement of Tibet due to the

Indo-Eurasian plate collision (Li et al. [30]). To further north, lie the Tian Shan ranges with numerous thrust faults trending in the east-west direction.

5. Kirthar-Sulaiman Ranges

The Himalayan arc trending NW-SE in the western portion bends stridently to south, while forming the Hazara-Kashmir syntaxis. The Sulaiman-Kirthar ranges originate here and traverse a length of nearly 1000 km in the north-south direction. These ranges may be described as a complex fold and thrust belt with numerous active strike-slip, dip-slip, and oblique-slip faults, which occasionally produce shallow and destructive earthquakes. The prominent features in these ranges include salt-range thrust Jhelum fault, and Kalabagh fault.

6. Indo-Gangetic Plain

The Indo-Gangetic plain are tectonically unmodified, youngest deposits at the foothills of the Himalayas. The moderate seismicity in this region is due to the Himalayan tectonics and the presence of several subsurface transverse features. The Mahendragarh-Dehradun fault (MDF), great boundary fault (GBF), Moradabad fault (MF), Delhi-Haridwar ridge (DHR), and Mathura fault (MF) are some of the notable features that contribute to the seismicity of this region (Gupta and Trifunac [31]).

COMPILATION OF EARTHQUAKE CATALOGUE

To analyze the association of seismicity with the major tectonic features in the region under consideration, a comprehensive catalogue on the past earthquakes with magnitudes 3.5 or more is compiled from various published and other authentic sources (both indigenous and international) spanning the period 1501–2011. The major sources of the non-instrumental historical data for the period prior to 1890 are Oldham [32], Milne [33], Lee et al. [34], and Quittmeyer and Jacob [35]. The sources of early instrumental data for the period 1890–1964 include Gutenberg and Richter [36], Gutenberg [37], Rothé [38], and Quittmeyer and Jacob [35]. Many later publications have given improved locations and/or magnitudes of the significant historical and early instrumental earthquakes. The important ones among those considered are due to Abe [39], Abe and Noguchi [40, 41], Pacheco and Sykes [42], Engdahl and Villaseñor [43], Ambraseys [44], Ambraseys and Douglas [45], and Szeliga et al. [46]. The instrumental data for the period since 1965, as made available at http://www.isc.ac.uk/ by International Seismological Centre (ISC), UK, http://earthquake.usgs.gov/earthquakes/search/ by National Earthquake Information Center (NEIC), USGS, http://www.ncedc.org/cnss/ by Northern California Earthquake Data Center, and at http://www.globalcmt.org/ under the global centroid-moment-tensor (CMT) project, is used. In addition, the catalogues prepared by Indian Meteorological Department (IMD) and Raghukanth [47] are used for the events not covered in the above sources. The compiled catalog is thoroughly scrutinized to remove the duplicate events and to select the best possible values of magnitude, location, and focal depth, when multiple options are available from different sources. The catalog thus compiled contained a total of 24,383 events with magnitudes 3.5 or more for the period 1501–2011.

Depending on the information available in the various data sources used, the compiled catalog includes different types of magnitude (viz., M_L, M_S, m_B, and m_b) for different events. This is therefore homogenized by converting other types of magnitude into the moment magnitude M_W by using suitable empirical conversion relationships. For the period prior to 1965, the types of magnitude available include the local magnitude M_L, 20-s surface wave magnitude M_S, and the long-period body wave magnitude m_B. The hierarchy adopted to homogenize the catalogue for this period is to approximate M_W by M_S for the magnitudes greater than 6.5, get M_S from m_B for the magnitudes greater than or equal to 6.1 by using the relation $m_B = 0.63M_S + 2.5$ (Gutenberg and Richter [48]) and approximate the computed value as M_W, or use $M_W = 0.887M_L + 0.67$ (Chung and Bernreuter [49]) to get M_W from M_L for the magnitudes up to 6.5. For the modern instrumental period since 1964, the hierarchy followed to homogenize the earthquake magnitude is to use the conversion relation $M_W = 0.99M_S + 0.08$ (Scordilis [50]) for M_S greater than or equal to 6.2, use the relation $M_W = 0.85m_b + 1.03$ (Scordilis [50]) for $3.5 \le m_b \le 6.2$, or to use the conversion relation for M_L for the magnitudes up to 6.5, where m_b represents the short-period body wave magnitude.

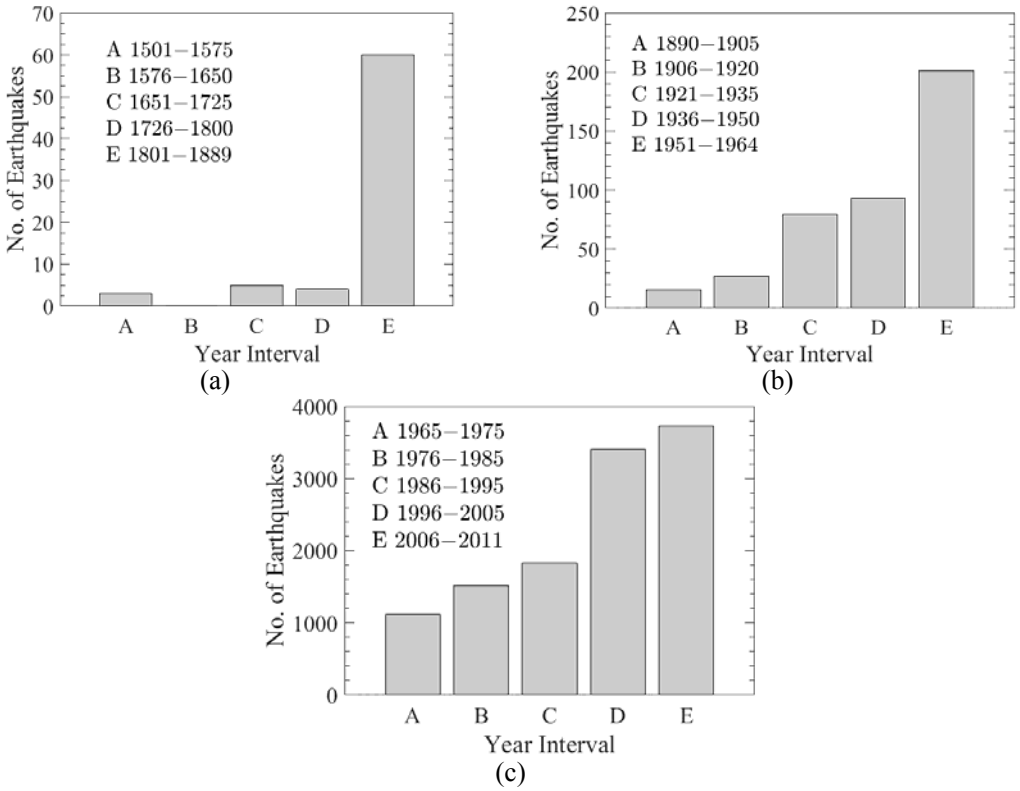

Fig. 2 Temporal distributions of events in earthquake catalogue in the periods (a) 1501–1889, (b) 1890–1964, and (c) 1965–2011

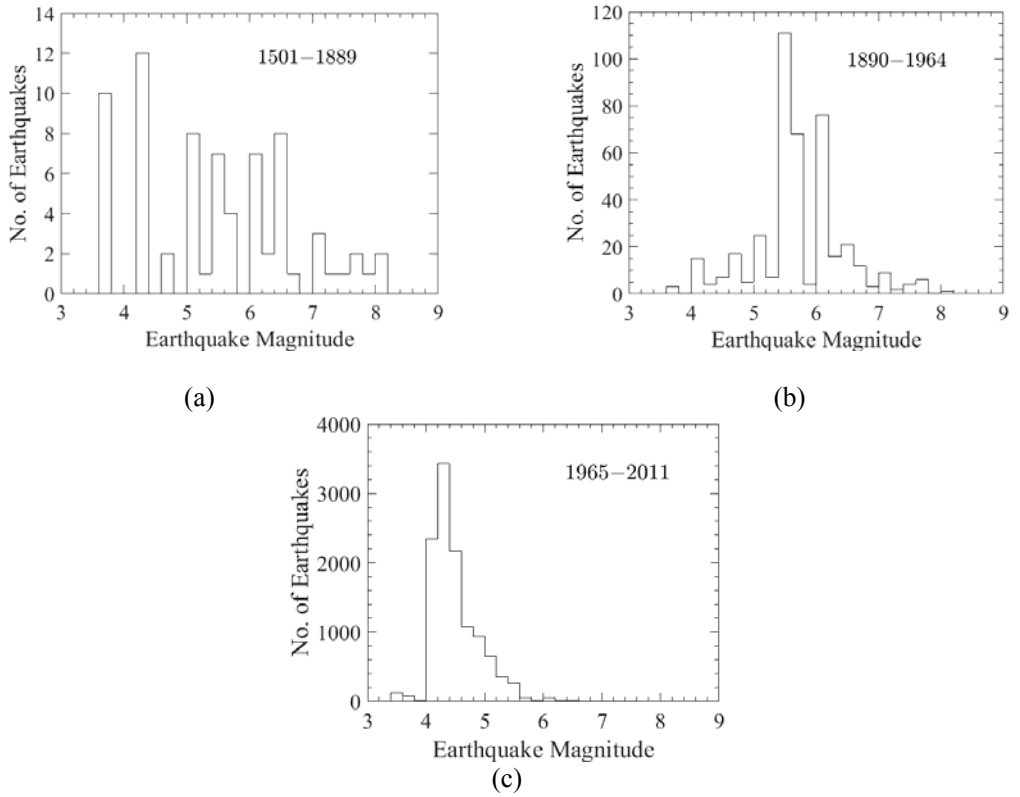

Fig. 3 Distributions over different magnitude intervals for events in earthquake catalogue in the periods (a) 1501–1889, (b) 1890–1964, and (c) 1965–2011

The homogenized catalogue is declustered to have only the main shocks by removing the foreshocks and aftershocks, such that the assumption made in PSHA that earthquakes follow a stationary Poisson process is satisfied. The window method proposed by Gardner and Knopoff [51] with the distance and time windows due to Uhrhammer [52] is used for this purpose. The declustering removes about 24.8% of the events, with 18,339 main events remaining for the present study.

In order to have an idea about the temporal distribution of events in the homogenized and declustered catalog, the histograms for the number of events over different time intervals are shown in Figure 2 for the periods 1501–1889, 1890–1964, and 1965–2011. It may be observed that fewer earthquakes are included in the catalogue as we go back in time, and thus the data may have to be considered incomplete before certain cut-off year, depending on the lower threshold magnitude. Figure 3 shows the histograms for the distributions of events over different magnitude intervals for the periods 1501–1889, 1890–1964, and 1965–2011. A very large number of events with the magnitudes between 4 and 6 are seen to have been reported during the period 1965–2011, most of which have occurred during the last 15 years.

Figure 4 shows the distribution over different focal depth intervals, which indicates that the region is frequented by both shallow-focus events (with focal depths less than 40 km) and intermediate-focus events (with focal depths up to 300 km). The shallow-focus events are mostly crustal earthquakes taking place around the Himalayan thrusts due to the interaction of continental plates, whereas the intermediate-focus events are centered at the Hindukush-Pamir subduction zone. It may be mentioned that there is a large number of earthquakes for which no information on focal depths is available and that most of these events belong to the historical period.

SEISMIC SOURCE ZONES AND THEIR SEISMICITY

The delineation of possible seismic source zones and the estimation of their seismicity in terms of expected occurrence rates of different magnitudes of earthquakes form an important part of the hazard analysis process. In an ideal situation, all the seismic sources have to be specific fault planes only, but this is not feasible in practice because all the faults in a region are generally not known and the past earthquakes are not seen to correlate closely with the known faults. Therefore, the broad area type of seismic sources of diffused seismicity is commonly assumed in practical applications. In order to identify various seismic sources in the present study, the epicenters of 12,089 main shocks with magnitudes 5.0 or more are plotted in Figure 5 over the tectonic map of Figure 1. Though the epicenters are seen to follow broadly the trends of major tectonic features in the region, those are scattered very widely and cannot be associated with specific faults. Also, it is not sure that all the faults in the northwestern Himalayan region under consideration are known, which makes it difficult to define individual fault plane type of seismic sources for the region. Therefore, it is decided to resort to the area sources with somewhat subjectively chosen boundaries. However, due to a non-uniform spatial distribution of the seismicity used in each source zone and the use of fault rupture dimensions in defining the source-to-site distance, with the rupture permitted to cross the source boundary, the subjectivity in delineating the source zones is not expected to crucially affect the hazard estimates in this study.

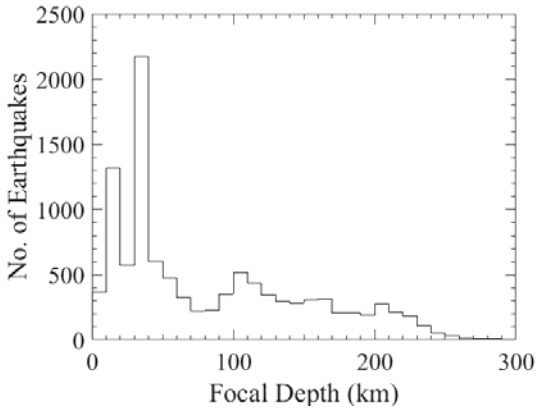

Fig. 4 Distribution over different focal depth intervals for events in earthquake catalogue

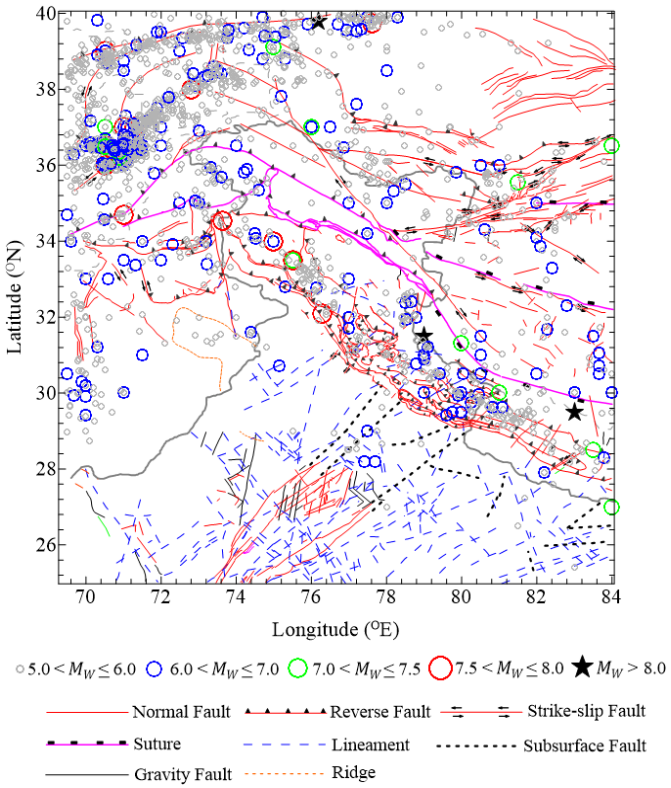

Fig. 5 Epicenters of past earthquakes in north-west Himalayas and adjoining region superimposed over the tectonic features

1. Delineation of Seismic Sources

A total of 16 area type sources of shallow crustal seismicity with arbitrary shapes, and one dipping planar source corresponding to the Hindukush subduction zone are identified for the region of study, as indicated in Figure 6 on the seismotectonic map of the region. The area sources are numbered as 1, 2, and 4–17, each one of which is characterized by a different level of seismicity in terms of the frequency of earthquakes as well as the maximum potential, and encompasses several faults and other stress-relieving geological features with the same type of predominant focal mechanism. The Hindukush deep subduction source zone is numbered as 3.

Starting with the northwest corner, Source 1 covers the north of Pamir and the Tian Shan block, and includes several major faults like the Main Pamir thrust and Darvaz fault. This region has been plagued by several shallow crustal earthquakes along the main Pamir thrust fault and other seismically active faults. The extreme northeast corner of the region is demarcated as Source 2, which comprises a significant part of the Tarim basin of China. This is a rigid block with little internal deformations or seismicity (Avouac et al. [53]; Yang and Liu [54]).

Sources 4 and 5 represent the Karakoram and western Tibetan regions, respectively. Both of these sources are characterized by quite high levels of seismicity related to the Karakorum fault system, and the major left-lateral strike-slip faults like the Karakax fault (which is a continuation of the Altyn Tagh fault to the west) and Kun Lun thrust fault. Sources 6 and 7 are defined around the main Karakoram thrust (MKT) and main mantle thrust (MMT) faults, while encompassing the areas of the Kohistan-Nanga Parbat and Ladakh blocks, respectively. Source 6 is characterized by marked changes in the trends of all the major tectonic features from northwest to southwest, thus making it a complex and tectonically active area. Source 8 encompasses the area of the Lhasa block between the Bangong Nujang and Indo-Tsangpo suture zones.

Source 9 represents the Hazara-Kashmir syntaxis, where the single most potent source in the Himalayas, i.e., MBT takes a hair pin turn. The Jhelum fault, which is a young fault dislocating MBT at

the syntaxis, is also quite active in this source. The Himalayan tectonic belt to the east is demarcated into Sources 10, 11, 12, and 13 on the basis of marked changes in the levels of seismicity and segmentation of Himalayas by the transverse faults. The thrusting movement along the mega thrusts like MBT, MCT, and MFT mainly contributes to the seismicity of these sources, which have been the hosts to several devastating earthquakes.

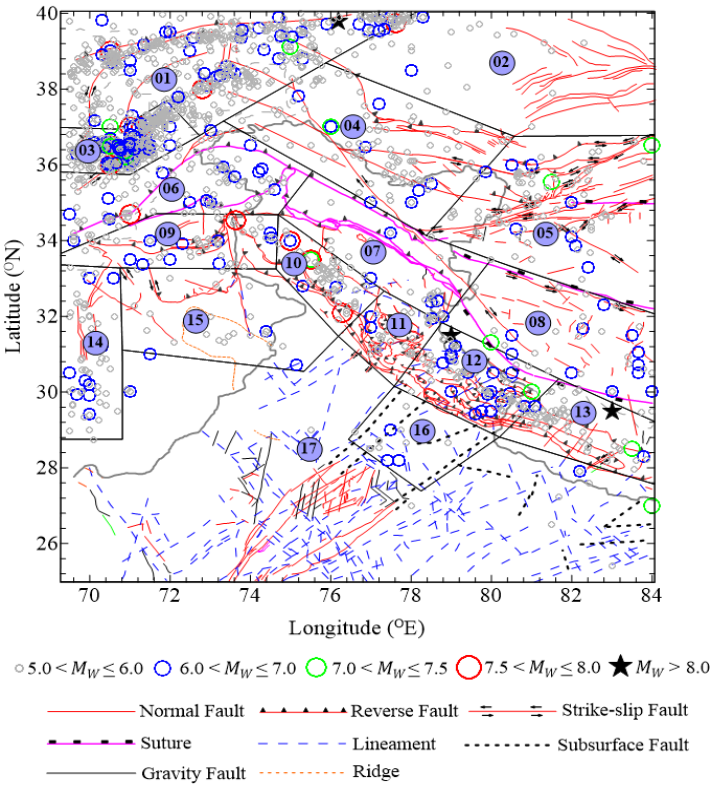

Fig. 6 The 17 seismic sources identified in north-west Himalayas and adjoining region

The western boundary of the Indian plate defined by the Chaman fault and Kirthar-Sulaiman ranges in Pakistan is taken as Source 14. Source 15 encapsulates the salt range region and the faults within. Source 16 is a moderately active source, defined to include the sub-surface features which prod into the Himalayan arc in the outer zone of foredeep in the Indo-Gangetic plain. The last area source, Source 17, is a very large size source having low level of seismicity and enclosing all the haphazardly spread lineaments in the Indo-Gangetic plain.

The deep subduction zone, Source 3, is a dipping plane source. This represents the Benioff zone of the Hindukush-Pamir knot area, which is a junction of several tectonic features. This source has an intense seismic activity characterized by a significant clustering of epicenters, which can be associated with the near vertical subduction of the north-western tip of the Indian plate under the Eurasian plate. Though this source zone is located far away from the Indian region, large earthquakes in this source can produce significant contributions to long-period ground motions in the northwest India.

Table 1 lists all the 17 sources by assigning a name to each source based on its geographic location, for a convenient identification in the description. The prominent tectonic features contained within each source, along with the preferred dip angle and predominant range of strike, are also given in Table 1. The range of strike is based on the general trend of tectonic features and epicenters of past earthquakes in the source, whereas the dip angle is defined by a preferred value from the seismological depth sections and/or available fault plane solutions.

Table 1: List of the 17 seismic sources identified in the northwest Himalayan region with source numbers, names assigned, prominent tectonic features hosted, preferred dip angles, and the expected ranges of strike

Source No.	Name of Source	Prominent Tectonic Features	Dip Angle (°)	Range of Strike (°)
1	Pamir-Tian Shan block	Main Pamir thrust, Darvez thrust, and Panjshir fault	40	250–275
2	Tarim basin	Tazhong fault system, and Madong fault system	40	270 (fixed)
3	Hindukush subduction	Hindukush Benioff zone	70	—
4	Karakoram area	Karakorum fault zone	25	260–290
5	Kunlun and western Tibet area	Kashitashi thrust, Karakax fault, and Kunlun thrust	90	230–290
6	Kohistan-Nanga Parbat area	Main Karakorum thrust, and main mantle thrust	40	220–270
7	Ladakh block	Main mantle thrust	40	290–310
8	Lhasa block	Bangong Nujiang and Indo-Tsangpo suture zones	90	280–310
9	Himalayan syntaxial zone	MBT thrust system	40	220–270
10	Western Himalayas-I	Himalayan thrusts (MFT, MBT and MCT)	25	280–320
11	Western Himalayas-II	Himalayan thrusts (MFT, MBT and MCT)	25	280–320
12	Western Himalayas-III	Himalayan thrusts (MFT, MBT and MCT)	25	270–310
13	Western Nepal Himalayas	Himalayan thrusts (MFT, MBT and MCT)	25	290–310
14	Western plate boundary	Chaman fault, and Kirthar ranges	40	180 (fixed)
15	Salt range area	Salt range thrust, and Kalabagh fault	40	250–260
16	Delhi-Hardwar ridge	Mahendragarh-Dehradun fault, Moradabad fault, and great boundary fault	70	40–60
17	Indo-Gangetic plain	System of lineaments	40	250–290

2. Modeling of Seismicity of Sources

The hazard computations require the estimation of the seismicity of each seismic source in terms of the expected occurrence rates of earthquakes of different magnitudes. This is achieved by defining an appropriate recurrence relationship with an upper bound maximum magnitude. For this purpose, it is necessary to first define for each source the following form of G-R relationship with no upper bound magnitude (Richter [15])

$$\log N(M) = a - bM \tag{1}$$

In this relationship, $N(M)$ is the occurrence rate of earthquakes with magnitudes equal to or greater than M, and a and b are the constants specific to each seismic source zone. Past earthquake data from the homogenized and declustered catalogue described above is used to estimate the parameters a and b by using the maximum likelihood method of Weichert [55], which utilizes the data in different magnitude ranges only for the periods, for which those have been reported completely. There are a large number of methods available in the literature (e.g., Stepp [56]; Tinti and Mulargia [57]; Woessner and Wiemer [58]; Albarello et al. [59]; Rotondi and Garavaglia [60]; Hainzl et al. [61]; Herak et al. [62]; Hakimhashemi and Grünthal [63]; etc.) for the purpose of completeness analysis, with each method requiring some degree of subjectivity. In this study the widely used Stepp's method (Stepp [56]) is employed, which is based on the stability of the occurrence rate of earthquakes in a given magnitude range with increase in time from present to the past.

2.1 Completeness Analysis

In order to estimate the periods of completeness by Stepp's method, the earthquake data for the source under consideration is grouped into several magnitude bins, and the average number of events per year, $R(M)$, is evaluated for different lengths of time, L, measured backwards from the present for each magnitude bin. Assuming Poisson distribution, Stepp [56] defined the standard deviation $S(R)$ of $R(M)$ as

$$S(R) = \sqrt{\frac{R(M)}{L}} \tag{2}$$

For the period of completeness, $R(M)$ is expected to be approximately constant, making $S(R)$ to vary as $1/\sqrt{L}$ with L. Thus, the period of completeness L_C for the magnitude bin under consideration is obtained by identifying the value of L, at which the trend of $R(M)$ deviates significantly from $1/\sqrt{L}$. This is achieved more conveniently on a logarithmic plot of $R(M)$ versus L, known as Stepp's completeness plot, wherein the departure in trend will correspond to a slope markedly different from $-1/2$.

The completeness plots for all the 17 source zones are shown in Figure 7, where the identified periods of completeness (corresponding to different magnitude bins) are also indicated for each source. For some of the source zones, it is not possible to identify the periods of completeness (from the completeness plots) in the case of bins involving very large magnitudes. For these bins, the periods of completeness might have exceeded the period covered by the catalogue. In these cases the completeness periods are arrived at by trials, such that the chosen periods lead to a smooth variation of $N(M)$ in accordance with the G-R relationship. The so-obtained completeness periods for all the seismic sources in different magnitude ranges are given in Table 2, with the periods that could not be decided from Stepp's plots indicated by asterisks.

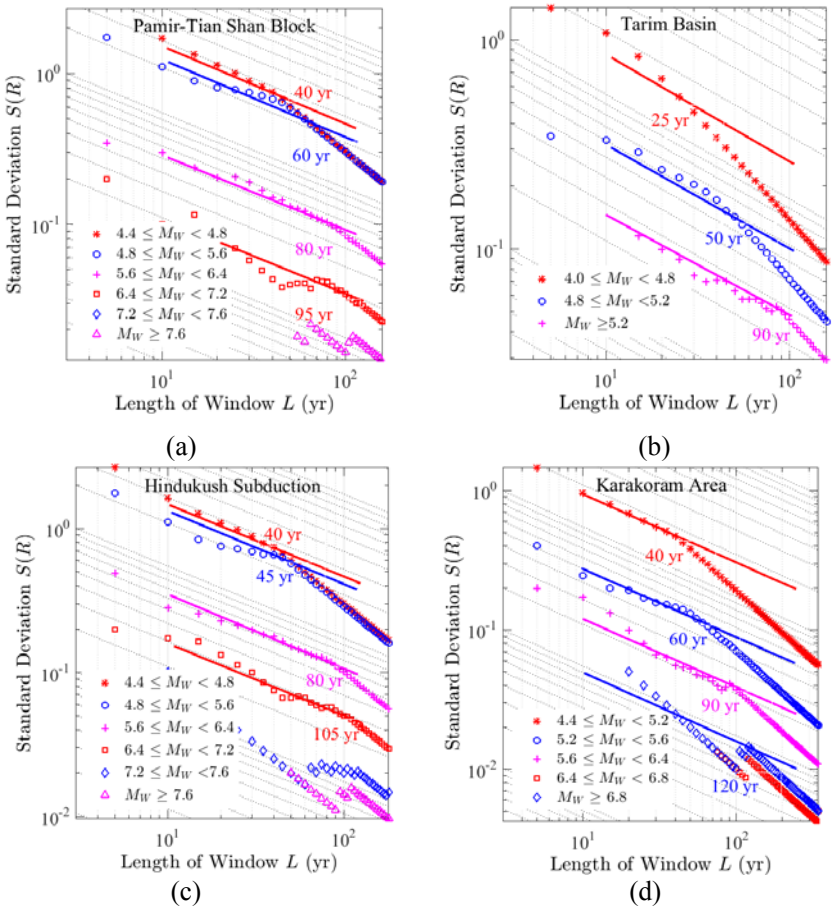

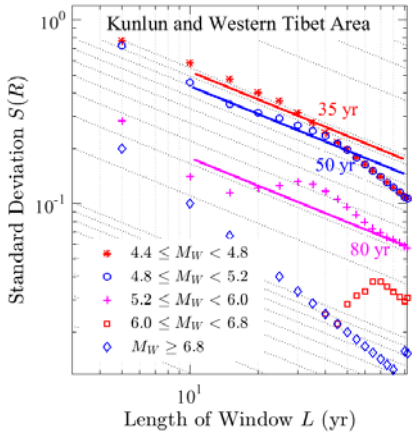
Kunlun and Western Tibet Area
35 yr
50 yr
80 yr
$4.4 \le M_W < 4.8$
$4.8 \le M_W < 5.2$
$5.2 \le M_W < 6.0$
$6.0 \le M_W < 6.8$
$M_W \ge 6.8$
Standard Deviation $S(R)$
Length of Window L (yr)

(e)

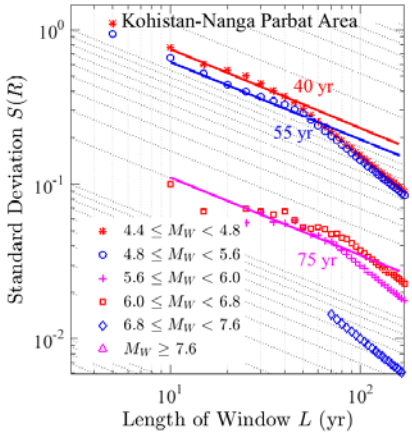
Kohistan-Nanga Parbat Area
40 yr
55 yr
75 yr
$4.4 \le M_W < 4.8$
$4.8 \le M_W < 5.6$
$5.6 \le M_W < 6.0$
$6.0 \le M_W < 6.8$
$6.8 \le M_W < 7.6$
$M_W \ge 7.6$
Standard Deviation $S(R)$
Length of Window L (yr)

(f)

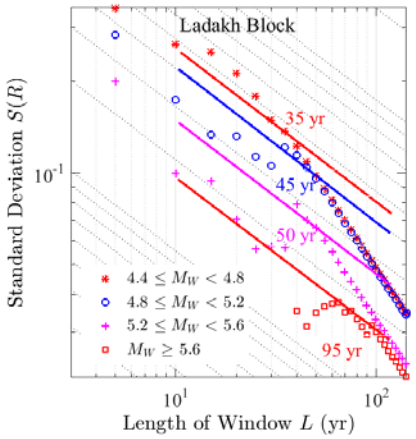
Ladakh Block
35 yr
45 yr
50 yr
95 yr
$4.4 \le M_W < 4.8$
$4.8 \le M_W < 5.2$
$5.2 \le M_W < 5.6$
$M_W \ge 5.6$
Standard Deviation $S(R)$
Length of Window L (yr)

(g)

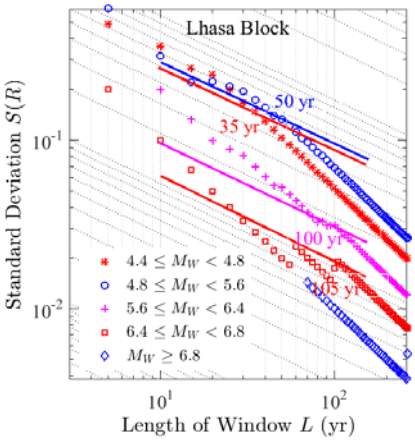
Lhasa Block
50 yr
35 yr
100 yr
75 yr
$4.4 \le M_W < 4.8$
$4.8 \le M_W < 5.6$
$5.6 \le M_W < 6.4$
$6.4 \le M_W < 6.8$
$M_W \ge 6.8$
Standard Deviation $S(R)$
Length of Window L (yr)

(h)

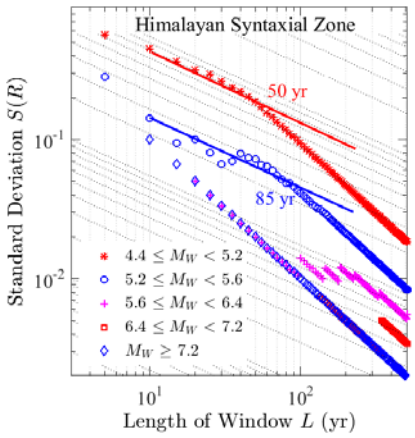
Himalayan Syntaxial Zone
50 yr
85 yr
$4.4 \le M_W < 5.2$
$5.2 \le M_W < 5.6$
$5.6 \le M_W < 6.4$
$6.4 \le M_W < 7.2$
$M_W \ge 7.2$
Standard Deviation $S(R)$
Length of Window L (yr)

(i)

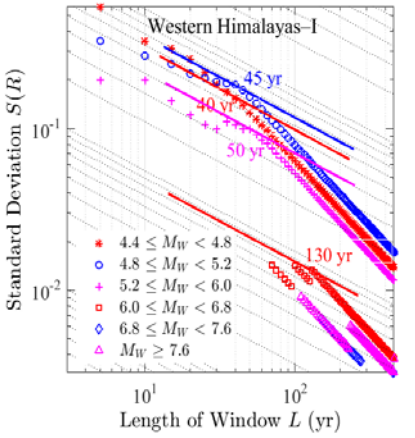
Western Himalayas–I
45 yr
40 yr
50 yr
130 yr
$4.4 \le M_W < 4.8$
$4.8 \le M_W < 5.2$
$5.2 \le M_W < 6.0$
$6.0 \le M_W < 6.8$
$6.8 \le M_W < 7.6$
$M_W \ge 7.6$
Standard Deviation $S(R)$
Length of Window L (yr)

(j)

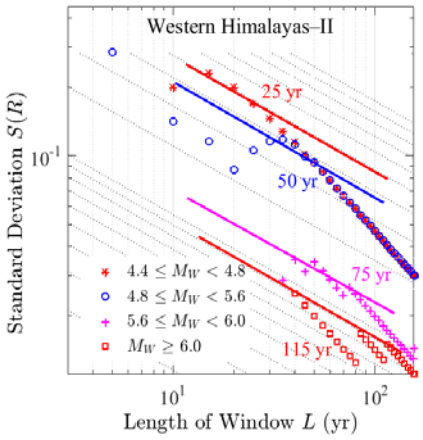
Western Himalayas–II
25 yr
50 yr
75 yr
115 yr
4.4 ≤ M_W < 4.8
4.8 ≤ M_W < 5.6
5.6 ≤ M_W < 6.0
M_W ≥ 6.0
Standard Deviation $S(R)$
Length of Window L (yr)

(k)

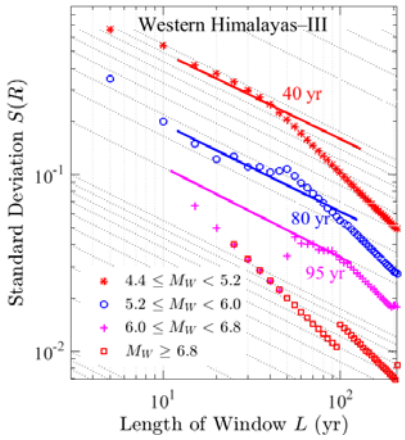
Western Himalayas–III
40 yr
80 yr
95 yr
4.4 ≤ M_W < 5.2
5.2 ≤ M_W < 6.0
6.0 ≤ M_W < 6.8
M_W ≥ 6.8
Standard Deviation $S(R)$
Length of Window L (yr)

(l)

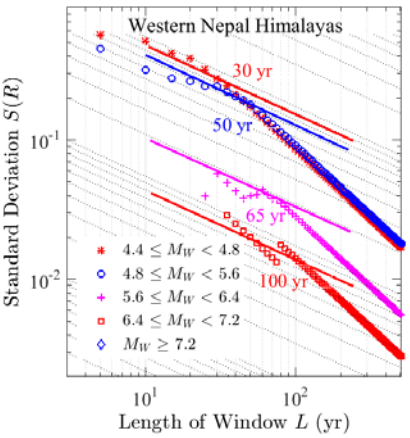
Western Nepal Himalayas
30 yr
50 yr
65 yr
100 yr
4.4 ≤ M_W < 4.8
4.8 ≤ M_W < 5.6
5.6 ≤ M_W < 6.4
6.4 ≤ M_W < 7.2
M_W ≥ 7.2
Standard Deviation $S(R)$
Length of Window L (yr)

(m)

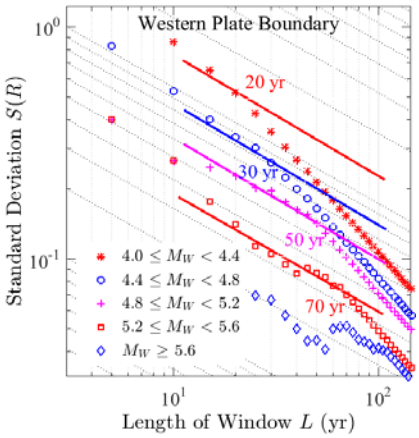
Western Plate Boundary
20 yr
30 yr
50 yr
70 yr
4.0 ≤ M_W < 4.4
4.4 ≤ M_W < 4.8
4.8 ≤ M_W < 5.2
5.2 ≤ M_W < 5.6
M_W ≥ 5.6
Standard Deviation $S(R)$
Length of Window L (yr)

(n)

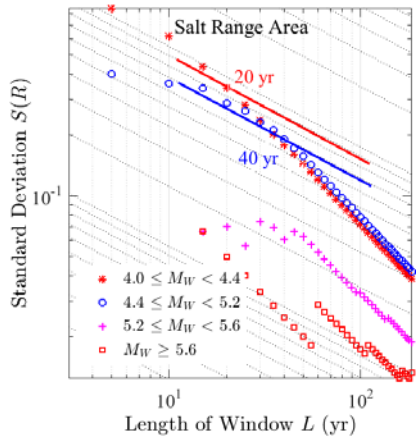
Salt Range Area
20 yr
40 yr
4.0 ≤ M_W < 4.4
4.4 ≤ M_W < 5.2
5.2 ≤ M_W < 5.6
M_W ≥ 5.6
Standard Deviation $S(R)$
Length of Window L (yr)

(o)

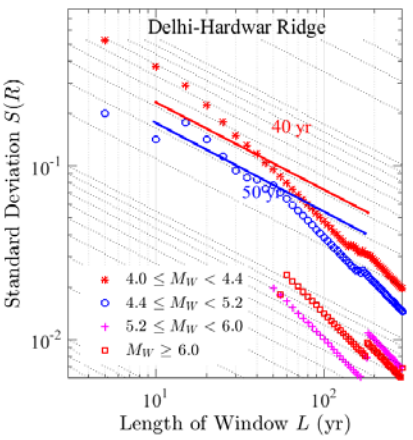
Delhi-Hardwar Ridge
40 yr
50 yr
4.0 ≤ M_W < 4.4
4.4 ≤ M_W < 5.2
5.2 ≤ M_W < 6.0
M_W ≥ 6.0
Standard Deviation $S(R)$
Length of Window L (yr)

(p)

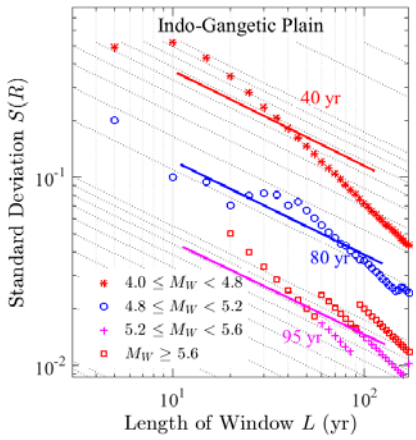

(q)

Fig. 7 $S(R)$ versus L plots for different magnitude bins in the cases of (a) Pamir-Tian Shan block, (b) Tarim basin, (c) Hindukush subduction, (d) Karakoram area, (e) Kunlun and western Tibet area, (f) Kohistan-Nanga Parbat area, (g) Ladakh block, (h) Lhasa block, (i) Himalayan syntaxial zone, (j) western Himalayas-I, (k) western Himalayas-II, (l) western Himalayas-III, (m) western Nepal Himalayas, (n) western plate boundary, (o) Salt range area, (p) Delhi-Hardwar ridge, and (q) Indo-Gangetic plain seismic sources (with the respective periods of completeness indicated)

Table 2: Periods of completeness for the identified seismic sources in different magnitude bins. Values with asterisks are decided by trial to achieve consistency with the occurrence rates for the smaller magnitude bins. Dashes indicate the magnitude bins to be beyond the upper bound magnitudes

Source No.	Name of Source	Magnitude Bin and Corresponding Completeness Period L_C (yr)						
1	Pamir-Tian Shan block	Mag. Bin	4.4–4.8	4.8–5.6	5.6–6.4	6.4–7.2	7.2–7.6	> 7.6
		L_C	40	60	80	95	145*	500*
2	Tarim basin	Mag. Bin	4.0–4.8	4.8–5.2	> 5.2	—	—	—
		L_C	25	50	90	—	—	—
3	Hindukush subduction	Mag. Bin	4.4–4.8	4.8–5.6	5.6–6.4	6.4–7.2	7.2–7.6	> 7.6
		L_C	40	45	85	105	210*	260*
4	Karakoram area	Mag. Bin	4.4–5.2	5.2–5.6	5.6–6.4	6.4–6.8	> 6.8	—
		L_C	40	60	90	120	350*	—
5	Kunlun and western Tibet	Mag. Bin	4.4–4.8	4.8–5.2	5.2–6.0	6.0–6.8	> 6.8	—
		L_C	35	50	80	95*	300*	—
6	Kohistan-Nanga Parbat area	Mag. Bin	4.4–4.8	4.8–5.6	5.6–6.0	6.0–6.8	6.8–7.6	> 7.6
		L_C	40	55	75	150*	170*	300*
7	Ladakh block	Mag. Bin	4.4–4.8	4.8–5.2	5.2–5.6	> 5.6	—	—
		L_C	35	45	50	95	—	—
8	Lhasa block	Mag. Bin	4.4–4.8	4.8–5.6	5.6–6.4	6.4–6.8	> 6.8	—
		L_C	35	50	100	105	265*	—
9	Himalayan syntaxial zone	Mag. Bin	4.4–5.2	5.2–5.6	5.6–6.4	6.4–7.2	> 7.2	—
		L_C	50	85	185*	345*	520*	—
10	Western Himalayas-I	Mag. Bin	4.4–4.8	4.8–5.2	5.2–6.0	6.0–6.8	6.8–7.6	> 7.6
		L_C	40	45	50	130	280*	500*
11	Western Himalayas-II	Mag. Bin	4.4–4.8	4.8–5.6	5.6–6.0	> 6.0	—	—
		L_C	25	50	75	115	—	—
12	Western	Mag. Bin	4.4–5.2	5.2–6.0	6.0–6.8	6.8	—	—

	Himalayas-III	L_C	40	80	95	300*	—	—
13	Western Nepal Himalayas	Mag. Bin	4.4–4.8	4.8–5.6	5.6–6.4	6.4–7.2	> 7.2	—
		L_C	30	50	65	100	510*	—
14	Western plate boundary	Mag. Bin	4.0–4.4	4.4–4.8	4.8–5.2	5.2–5.6	> 5.6	—
		L_C	20	30	50	70	145*	—
15	Salt range area	Mag. Bin	4.0–4.4	4.4–5.2	5.2–5.6	> 5.6	—	—
		L_C	20	40	140*	185*	—	—
16	Delhi-Hardwar ridge	Mag. Bin	4.0–4.4	4.4–5.2	5.2–6.0	> 6.0	—	—
		L_C	40	50	185*	300*	—	—
17	Indo-Gangetic plain	Mag. Bin	4.0–4.4	4.4–5.2	5.2–6.0	> 6.0	—	—
		L_C	40	80	95*	170*	—	—

2.2 Recurrence Models for Seismicity

The recurrence model of Equation (1) without an upper bound magnitude $M_{\max}$ may unrealistically overestimate the seismic hazard. Therefore, in practical hazard analysis applications, the recurrence model for a seismic source is defined while involving $M_{\max}$. Several alternative forms of the recurrence model can be considered, depending on whether $M_{\max}$ is imposed on the cumulative form of the G-R relation of Equation (1) or on the corresponding density function (Anderson [64]). In this study the following widely used form of recurrence model is adopted (Page [65]; Cornell and Vanmarcke [66]):

$$N(M) = N(M_{\min})\frac{e^{-\beta M} - e^{-\beta M_{\max}}}{e^{-\beta M_{\min}} - e^{-\beta M_{\max}}}; \quad \text{with } \beta = b\ln 10 \tag{3}$$

Here, $N(M_{\min})$ is the number of earthquakes with magnitudes greater than or equal to a minimum magnitude $M_{\min}$, which for each source zone is obtained from Equation (1). The choice of $M_{\min}$ is not very crucial in defining the recurrence relation of Equation (3). However, the lower threshold magnitude used for hazard computations should neither be too small nor very large, and should therefore be chosen judiciously (Bommer and Crowley [67]).

The parameters a, b (or β) (with respective standard deviations), and $M_{\max}$ required to define the recurrence relation of Equation (3), and the number of earthquakes used to estimate these parameters are listed for all the 17 source zones in the region of study in Table 3. The parameters a and b are determined by using the maximum likelihood method of Weichert [55] on the data for different magnitude intervals within the respective periods of completeness in a seismic source. However, the value of $M_{\max}$ for a source zone depends in a very complex manner on the tectonics and seismic history in the long geological past. In the absence of a precise knowledge of these factors in real applications, a lot of subjectivity is involved in the methods available for the estimation of $M_{\max}$ (Wheeler [68]). Since the observed maximum magnitude in a source can be considered to provide a lower bound to $M_{\max}$, the $M_{\max}$ values are assigned in this study by judiciously enhancing the observed maximum magnitude in each of the source zones. Even though mathematical formulations are available to estimate such an increment (Kijko and Singh [69]), appropriate increments are assumed here, while considering the widely accepted regional seismic potential, and the available seismic data for each source.

Figure 8 shows the recurrence model of Equation (3) fitted to the observed data in the 17 source zones considered in the present study. Also shown in each plot are the error bars corresponding to the interval of one standard deviation above and below the observed cumulative occurrence rates. It may be observed that all the recurrence curves pass through the error bars in more than 2/3rd cases, which is considered to be a reasonably good fitting of the model with the data points (Weichert [55]).

Table 3: Recurrence parameters *a* and *b* along with the associated standard deviations, the numbers of earthquakes, and the maximum magnitudes, M_{max}, based on the observed maximum magnitudes, M_{max}^{obs}, for the identified seismic sources

Source No.	Name of Source	*a*	*b*	M_{max}^{obs}	M_{max}	No. of Earthquakes
1	Pamir-Tian Shan block	6.63±0.13	1.14±0.03	8.1	8.5	3139
2	Tarim basin	5.63±0.24	1.17±0.06	6.2	6.5	276
3	Hindukush subduction	6.25±0.09	1.05±0.02	7.8	8.3	4317
4	Karakoram area	6.14±0.22	1.18±0.05	7.1	7.6	902
5	Kunlun and western Tibet area	5.63±0.26	1.12±0.06	7.2	7.7	450
6	Kohistan-Nanga Parbat area	6.09±0.18	1.16±0.04	7.6	8.0	974
7	Ladakh block	3.61±0.48	0.78±0.11	6.3	7.0	128
8	Lhasa block	4.00±0.30	0.85±0.07	7.0	7.5	201
9	Himalayan syntaxial zone	5.02±0.30	1.08±0.07	7.6	8.0	231
10	Western Himalayas-I	4.39±0.22	0.90±0.05	7.9	8.5	261
11	Western Himalayas-II	4.25±0.61	0.94±0.14	6.2	7.0	98
12	Western Himalayas-III	4.47±0.22	0.91±0.05	8.1	8.5	244
13	Western Nepal Himalayas	5.17±0.26	1.04±0.06	8.2	8.5	287
14	Western plate boundary	5.04±0.20	1.02±0.05	6.4	6.6	285
15	Salt range area	5.15±0.28	1.14±0.07	6.5	6.7	140
16	Delhi-Hardwar ridge	3.96±0.44	1.01±0.11	6.5	6.7	70
17	Indo-Gangetic plain	4.62±0.40	1.11±0.11	6.0	6.3	85

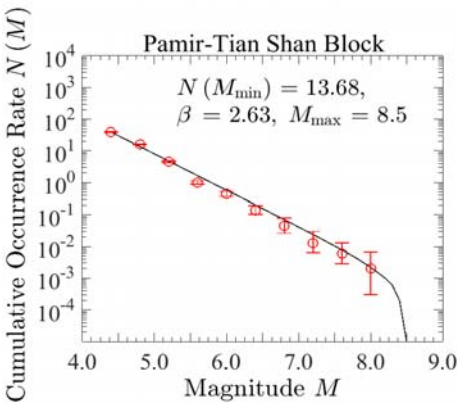

(a)

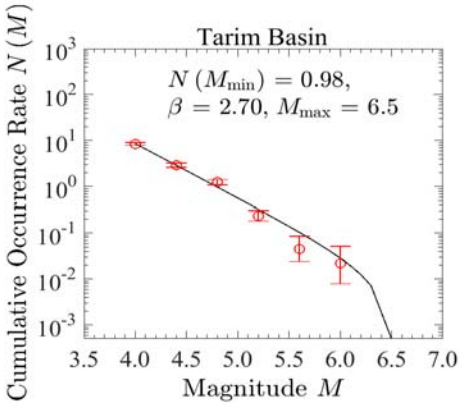

(b)

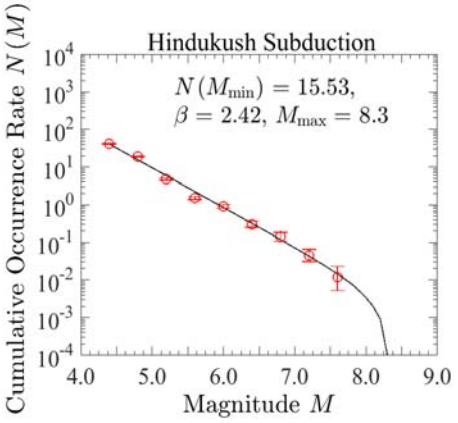

(c)

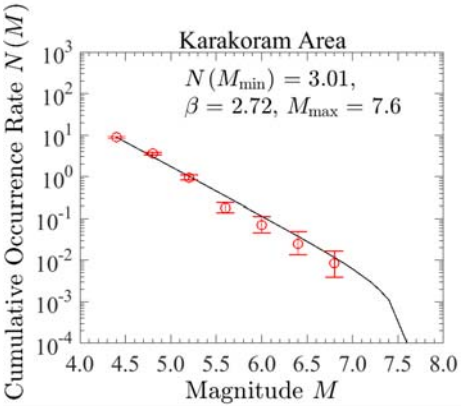

(d)

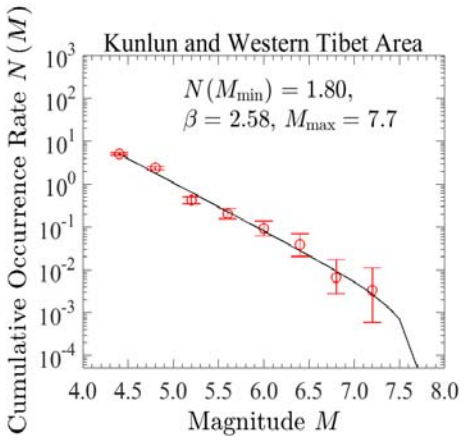
Kunlun and Western Tibet Area
$N(M_{\min}) = 1.80$,
$\beta = 2.58$, $M_{\max} = 7.7$
Cumulative Occurrence Rate $N(M)$
Magnitude M

(e)

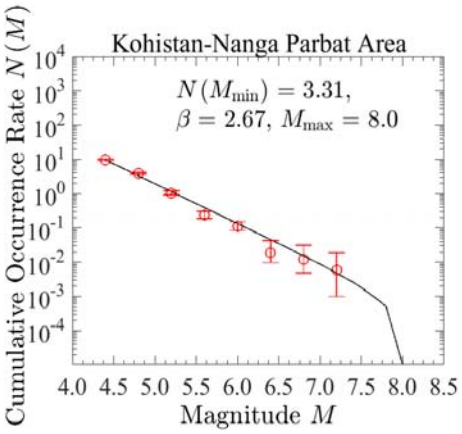
Kohistan-Nanga Parbat Area
$N(M_{\min}) = 3.31$,
$\beta = 2.67$, $M_{\max} = 8.0$
Cumulative Occurrence Rate $N(M)$
Magnitude M

(f)

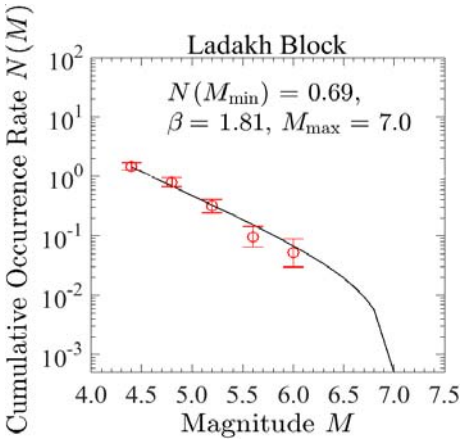
Ladakh Block
$N(M_{\min}) = 0.69$,
$\beta = 1.81$, $M_{\max} = 7.0$
Cumulative Occurrence Rate $N(M)$
Magnitude M

(g)

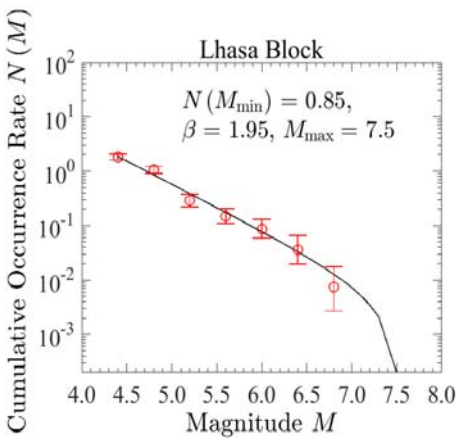
Lhasa Block
$N(M_{\min}) = 0.85$,
$\beta = 1.95$, $M_{\max} = 7.5$
Cumulative Occurrence Rate $N(M)$
Magnitude M

(h)

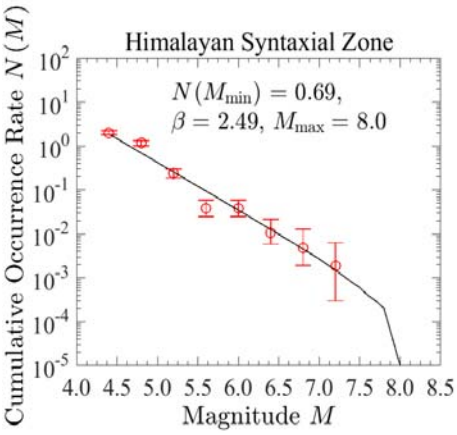
Himalayan Syntaxial Zone
$N(M_{\min}) = 0.69$,
$\beta = 2.49$, $M_{\max} = 8.0$
Cumulative Occurrence Rate $N(M)$
Magnitude M

(i)

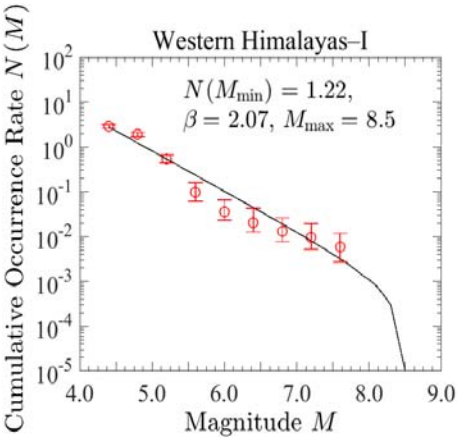
Western Himalayas–I
$N(M_{\min}) = 1.22$,
$\beta = 2.07$, $M_{\max} = 8.5$
Cumulative Occurrence Rate $N(M)$
Magnitude M

(j)

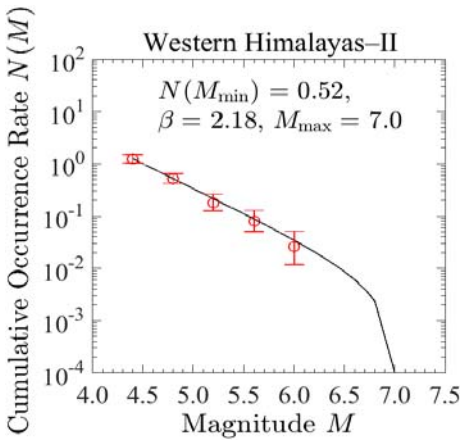
Western Himalayas–II
$N(M_{min}) = 0.52$,
$\beta = 2.18$, $M_{max} = 7.0$
Cumulative Occurrence Rate $N(M)$
Magnitude M

(k)

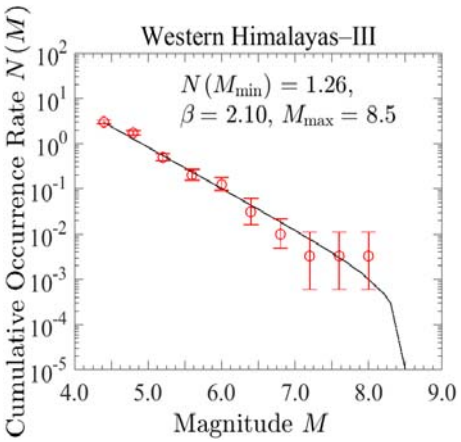
Western Himalayas–III
$N(M_{min}) = 1.26$,
$\beta = 2.10$, $M_{max} = 8.5$
Cumulative Occurrence Rate $N(M)$
Magnitude M

(l)

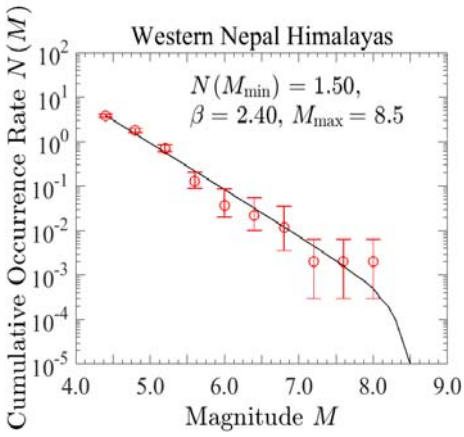
Western Nepal Himalayas
$N(M_{min}) = 1.50$,
$\beta = 2.40$, $M_{max} = 8.5$
Cumulative Occurrence Rate $N(M)$
Magnitude M

(m)

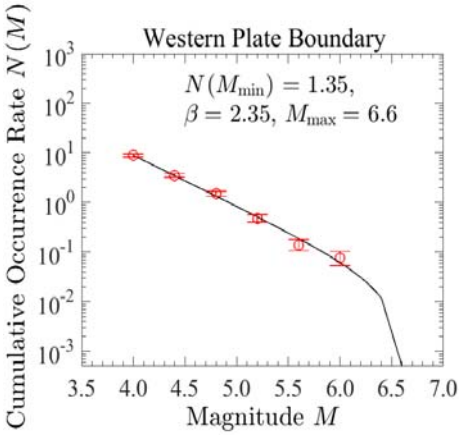
Western Plate Boundary
$N(M_{min}) = 1.35$,
$\beta = 2.35$, $M_{max} = 6.6$
Cumulative Occurrence Rate $N(M)$
Magnitude M

(n)

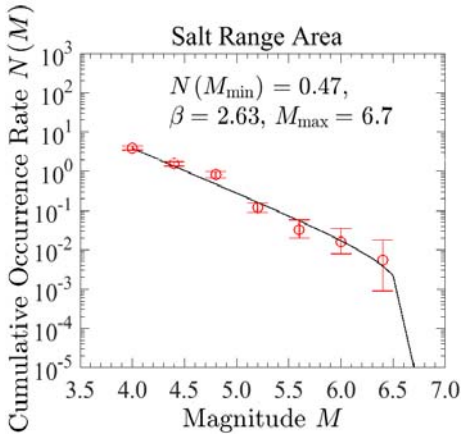
Salt Range Area
$N(M_{min}) = 0.47$,
$\beta = 2.63$, $M_{max} = 6.7$
Cumulative Occurrence Rate $N(M)$
Magnitude M

(o)

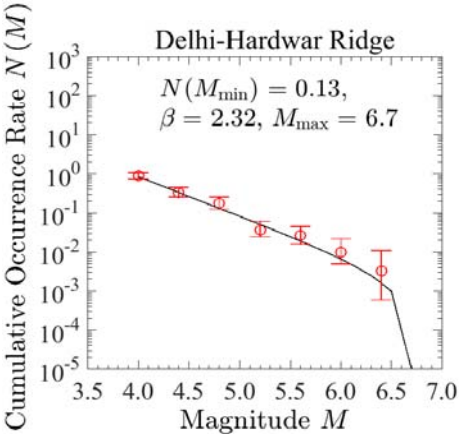
Delhi-Hardwar Ridge
$N(M_{min}) = 0.13$,
$\beta = 2.32$, $M_{max} = 6.7$
Cumulative Occurrence Rate $N(M)$
Magnitude M

(p)

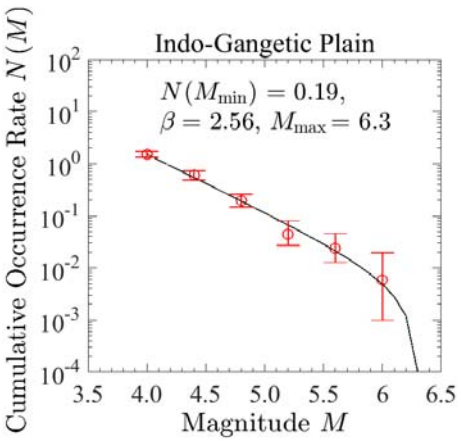

(q)

Fig. 8 Recurrence plots and error bars for $\pm$ standard deviation in the cases of (a) Pamir-Tian Shan block, (b) Tarim basin, (c) Hindukush subduction, (d) Karakoram area, (e) Kunlun and western Tibet area, (f) Kohistan-Nanga Parbat area, (g) Ladakh block, (h) Lhasa block, (i) Himalayan syntaxial zone, (j) western Himalayas-I, (k) western Himalayas-II, (l) western Himalayas-III, (m) western Nepal Himalayas, (n) western plate boundary, (o) Salt range area, (p) Delhi-Hardwar ridge, and (q) Indo-Gangetic plain seismic sources (with the corresponding values of $N(M_{\min})$, β, and $M_{\max}$ indicated)

SELECTION OF GROUND MOTION PREDICTION EQUATIONS

The results of a seismic hazard analysis depend strongly on the ground motion prediction equations (GMPEs) or attenuation relationships used, which have to be region-specific in order to obtain reliable and realistic estimates of the hazard. In order to get around the unintended subjectivity in the selection of suitable GMPEs in practical applications, Bommer et al. [70] proposed several qualitative selection criteria for making an initial choice of the relevant equations for a target region of interest. These criteria require that the selected equations have been developed for the regions with tectonic settings similar to those of the target region, that the magnitude and distance dependence in the selected equations are constrained in a physically realistic manner, that the datasets used for the selected equations cover an ample range of earthquake magnitudes and source-to-site distances without any significant gaps in between, and that the selected equations predict the spectral amplitudes (i.e., SA in the present study) for an adequate range of periods.

The final selection of GMPEs in the present study is made by conducting a performance evaluation of each equation shortlisted in the initial selection by using the limited strong-motion data available for the study region of western Himalayas and adjoining regions. In order that the performance evaluation is free from any possible bias due to personal judgment, a one-to-one comparison of the actual SA values corresponding to the recorded ground motions is made with the corresponding SA values predicted by the candidate equations, followed by a quantification of the extent of match in respect of the chosen goodness-of-fit measures. The candidate equation that gives the closest agreement of the actual and predicted SA values is selected as the suitable GMPE.

The goodness-of-fit measures employed here are based on the statistics of residuals that are calculated as the logarithms of the observed SA values subtracted by the predicted mean levels of the logarithm of SA. These residuals are normalized by the standard deviations, SD, specified by the candidate GMPE (for the logarithm of SA), such that the normalized residual, NR, for a pair of observed SA value, $\mathrm{SA}_{\mathrm{obs}}$, and predicted SA value, $\mathrm{SA}_{\mathrm{pre}}$, becomes equal to $\left(\ln \mathrm{SA}_{\mathrm{obs}} - \ln \mathrm{SA}_{\mathrm{pre}}\right)/\mathrm{SD}$. The normalized residuals are expected to follow the standard normal distribution (with mean equal to 0 and standard deviation equal to 1). Significant deviations in the mean and standard deviation of the actual distribution of these residuals from the values of 0 and 1, respectively, would indicate a poor matching. Another goodness-of-fit measure employed here is the likelihood-based measure proposed by

Scherbaum et al. [71], wherein an LH value is calculated for a NR value as the probability for the normalized residual to fall outside the interval of $-\mathrm{NR}$ and NR, i.e.,

$$\mathrm{LH} = \sqrt{\frac{2}{\pi}} \int_{|\mathrm{NR}|}^{\infty} \exp\left(-\frac{z^2}{2}\right) \mathrm{d}z \tag{4}$$

For a perfect matching of the standard deviation of the observed SA values with the standard deviation specified by the candidate GMPE, the LH values should be distributed uniformly between 0 and 1, with a median value of 0.5. The LH distribution becomes skewed to the left/right (with the median significantly less/more than 0.5), if the standard deviation specified by the candidate equation is less/more than the standard deviation of the observed SA values.

1. GMPE for Shallow Crustal Earthquakes

The 16 area-type seismic sources in the study region are characterized by the shallow crustal earthquakes. Six GMPEs are shortlisted in the initial selection for these sources based on the criteria of Bommer et al. [70] mentioned above. These equations have been proposed by Abrahamson and Silva [72], Boore and Atkinson [10], Campbell and Bozorgnia [73], Chiou and Youngs [74], Lee [75], and Sharma et al. [76]. Even though the first four of these equations have been updated under the NGA-West2 project and published in Volume 30, No. 3 issue of Earthquake Spectra in 2014, the updated versions are not considered in this study due to the difficulty in assigning reliable values to the additional input parameters involved. Further, the region-specific equations by Anbazhagan et al. [77] and Ramkrishnan et al. [78] are not considered because those do not consider the dependence on site conditions, and the latter one is only for PGA. Similarly, the relations by Gupta and Trifunac [79, 80] are also not considered because those are applicable to very limited period ranges with decreasing magnitude. The salient features of the six GMPEs considered are summarized in Table 4, including the regions for which those have been developed, their magnitude ranges of applicability, distance metrics involved in those, their distance ranges of applicability, their period ranges of applicability, and the parameters used for the site classification in those. All the six candidate equations give the estimates of the logarithm of SA at 5% damping for the horizontal motions.

Table 4: Particulars of the candidate GMPEs considered for shallow crustal earthquakes

S. No.	Candidate Equation	Host Region	Magnitude Range	Distance Metric	Distance Range (km)	Period Range (s)	Site Classification Parameter
1	Abrahamson and Silva [72]	Worldwide	5.0–8.5	R_{rup}	0–200	0–10	V_{S30}
2	Boore and Atkinson [10]	Worldwide	5.0–8.0	R_{jb}	0–200	0–10	V_{S30}
3	Campbell and Bozorgnia [73]	Worldwide	4.0–8.5	R_{rup}	0–200	0–10	V_{S30}
4	Chiou and Youngs [74]	Worldwide	4.0–8.5	R_{rup}	0–200	0–10	V_{S30}
5	Sharma et al. [76]	Indian Himalayas & Zagros region of Iran	5.5–6.8	R_{jb}	5–200	0.04–2.5	Qualitative (rock & soil)
6	Lee [75]	Mostly California region of USA	2.4–7.7	Equi-valent Distance	0–200	0.04–15	Qualitative (rock, stiff soil, and deep soil)

In order to estimate various distance measures involved in the candidate GMPEs, the rupture plane is idealized as a rectangle, with the hypocenter located at the centroid of the rectangle (Gupta [81]). The length L and width W of the rupture are estimated from the magnitude M_W by using the empirical relations given by Leonard [82]. The equations of Abrahamson and Silva [72] and Chiou and Youngs [74] also use a soil depth parameter, $Z_{1.0}$, representing the depth (in m) to the shear wave velocity of 1000 m/s. This parameter is estimated by using the empirical relation of Abrahamson and Silva [72] in terms of V_{S30}. Similarly, the equation of Campbell and Bozorgnia [73] uses the basin or sediment depth $Z_{2.5}$ (in m) to the shear wave velocity of 2500 m/s, which is estimated from the empirical relationship of Campbell and Bozorgnia [83] in terms of $Z_{1.0}$. Further, there are two flags to differentiate the type of faulting, and one flag for differentiating main shocks from aftershocks, in the candidate GMPEs. These flags are assigned suitable values with the help of the information available about the contributing earthquakes (Gupta [84]).

The performance evaluation of the six candidate GMPEs is conducted by using the 254 uniformly processed, baseline corrected, strong ground motion records from 84 recording stations due to 71 shallow crustal earthquakes as in Gupta [84]. The particulars of the 71 events and 84 stations are given in Jaisal [85]. The V_{S30} values for the recording stations are adopted from Mittal et al. [86], even though some of those appear to be unrealistically high, in the absence of any better alternative. Figure 9 shows the distribution of the 254 records with respect to magnitude M_W and epicentral distance R_e for different ranges of V_{S30} at the recording sites. It may be observed that a majority of data are for the earthquakes with magnitudes below 5.5. Only a few records are there for the earthquakes between the magnitudes 6 and 7. These records are for a distance range of within 200 km and are mostly from the sites with rock/stiff soil conditions (i.e., $V_{S30} > 1100$ m/s). The overall distribution of the 254 records with respect to distance and site soil conditions is however seen to cover all the ranges in a balanced manner.

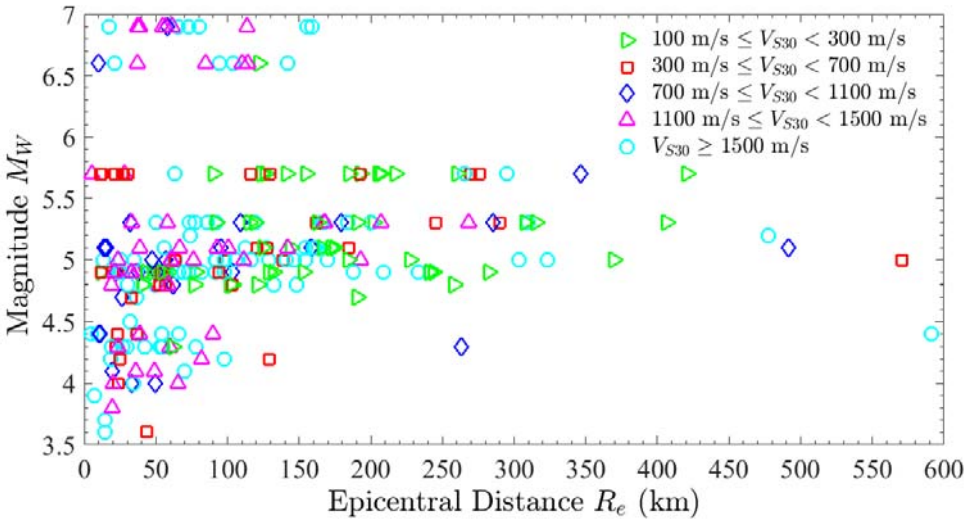

Fig. 9 Distribution of ground motion records for shallow crustal earthquakes with respect to magnitude M_W and epicentral distance R_e for different ranges of V_{S30} values at recording sites

The observed spectral amplitudes for each record are taken as the geometric mean of the SA values of the two horizontal components. Those are then used to compute the normalized residuals, NR, and the corresponding LH values at 17 natural periods of 0.01, 0.02, 0.03, 0.04, 0.05, 0.075, 0.1, 0.15, 0.2, 0.3, 0.4, 0.5, 0.75, 1.0, 1.5, 2.0, and 3.0 s for all the 254 records. Figures 10(a)–10(f) show the histograms of the so-obtained (254×17 =) 4318 NR and LH values for the candidate GMPEs by Abrahamson and Silva [72], Boore and Atkinson [10], Campbell and Bozorgnia [73], Chiou and Youngs [74], Lee [75], and Sharma et al. [76], respectively. Each plot for the NR values also shows the normal distribution fitted to the observed data together with the standard normal distribution for comparison. The computed goodness-of-fit measures, i.e., the mean and SD of normalized residuals NR, and the median of

LH values, are also indicated in each of Figures 10(a)–10(f) and listed for all six candidate GMPEs in Table 5. It may be observed that the matching between the actual distribution of the normalized residuals and the standard normal distribution varies from the worst for the GMPE by Sharma et al. [76] to the best for the GMPE by Abrahamson and Silva [72]. For the latter GMPE in particular, the mean is close to zero and SD is marginally greater than the value of 1. The LH values also appear to be most unevenly distributed in the case of the GMPE by Sharma et al. [76] and most evenly distributed in the case of the GMPE by Abrahamson and Silva [72]. For the latter GMPE in particular, the LH value distribution is skewed to the left with the median equal to 0.391, and thus the standard deviations specified for this GMPE are less than the standard deviations of the observed data at different periods.

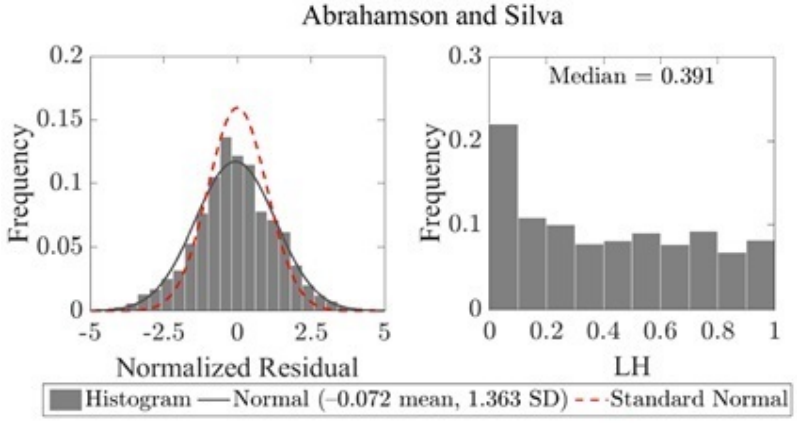

(a)

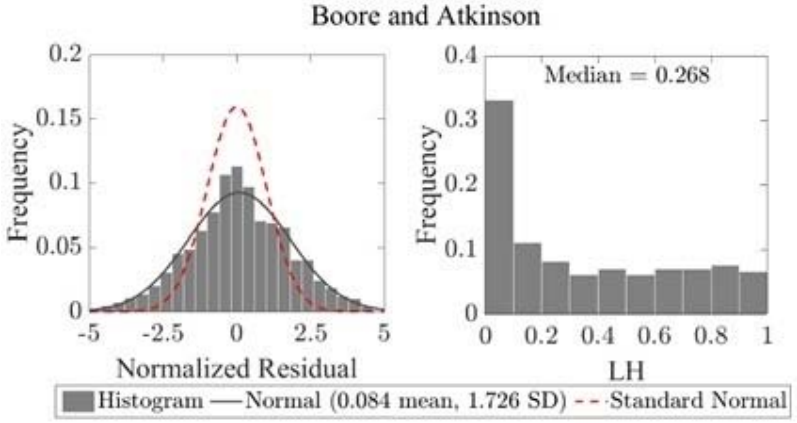

(b)

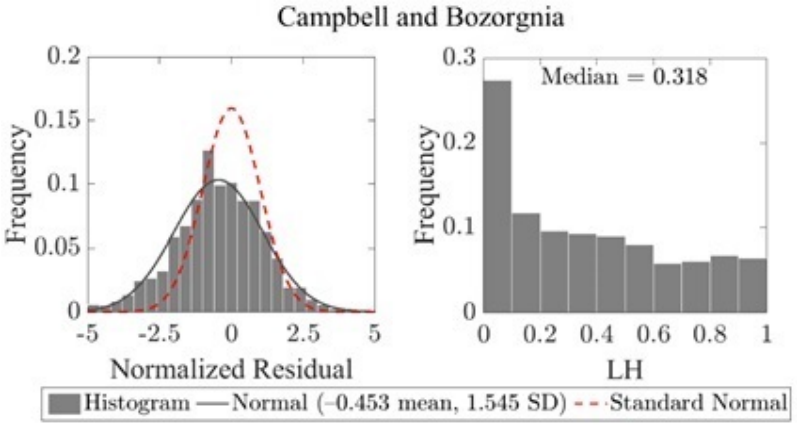

(c)

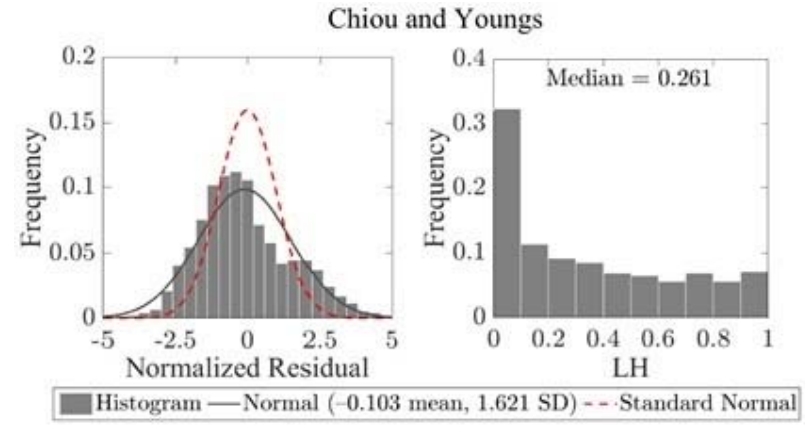

(d)

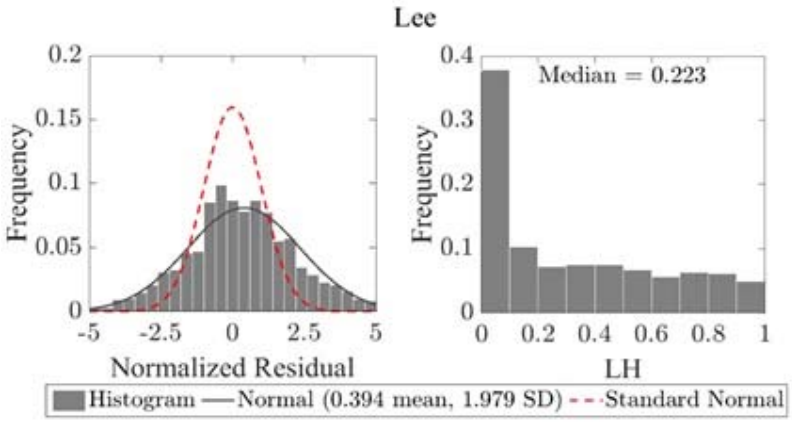

(e)

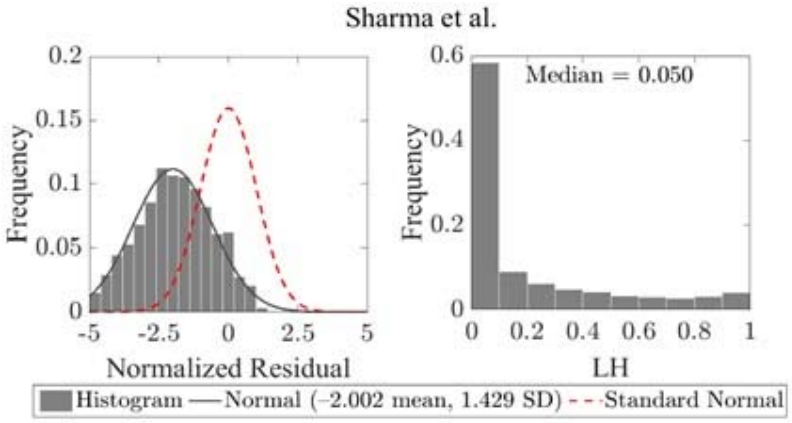

(f)

Fig. 10 (left) Comparison of the histograms of the normalized residuals, NR, and the best-fit normal distributions (solid curves; with the mean and SD values as indicated) with the standard normal distribution (dashed curves), and (right) the histograms of corresponding likelihood function LH values (with the median values indicated), for the candidate GMPEs by (a) Abrahamson and Silva [72], (b) Boore and Atkinson [10], (c) Campbell and Bozorgnia [73], (d) Chiou and Youngs [74], (e) Lee [75], and (f) Sharma et al. [76]

Table 5: Goodness-of-fit measures for the candidate GMPEs considered for shallow crustal earthquakes

Serial No.	Candidate GMPE	Mean of NR Values	SD of NR Values	Median of LH Values
1	Abrahamson and Silva [72]	−0.072	1.363	0.391
2	Boore and Atkinson [10]	0.084	1.726	0.268
3	Campbell and Bozorgnia [73]	−0.453	1.545	0.318
4	Chiou and Youngs [74]	−0.103	1.621	0.261
5	Lee [75]	0.394	1.979	0.223
6	Sharma et al. [76]	−2.002	1.429	0.050

The GMPE by Abrahamson and Silva [72] is considered to be the most appropriate GMPE for the present study despite the slight mismatch between the standard deviations. Scattering in the observed data may be too large due to the limited number of records, dominance of records with low signal-to-noise ratio (due to several smaller magnitude earthquakes), analog type of records with questionable quality for larger magnitude earthquakes, and 'too high' V_{S30} values taken from Mittal et al. [86]. The functional form of this GMPE consists of (i) a base model in terms of the moment magnitude M_W and the closest distance to the fault rupture area, R_{rup}, (ii) a nonlinear site-response model involving a continuous site soil characterization through the parameter, V_{S30}, (iii) a model for considering whether the site is on the hanging-wall or foot-wall side, as sites on the hanging-wall side experience larger motions (Abrahamson and Somerville [87]), (iv) a model for dependence on the depth to the top of fault rupture plane, as the buried ruptures lead to larger short-period ground motions (Somerville and Pitarka [88]), (v) a model for large-distance attenuation in the case of moderate earthquakes (i.e., when R_{rup} > 100 km), and (vi) a model for amplification due to the depth of soil at the site, which is characterized by $Z_{1.0}$, i.e., the depth at which shear wave velocity attains a value of 1.0 km/s. It also incorporates three terms with flags to differentiate between the types of faulting (i.e., reverse, normal, and strike-slip).

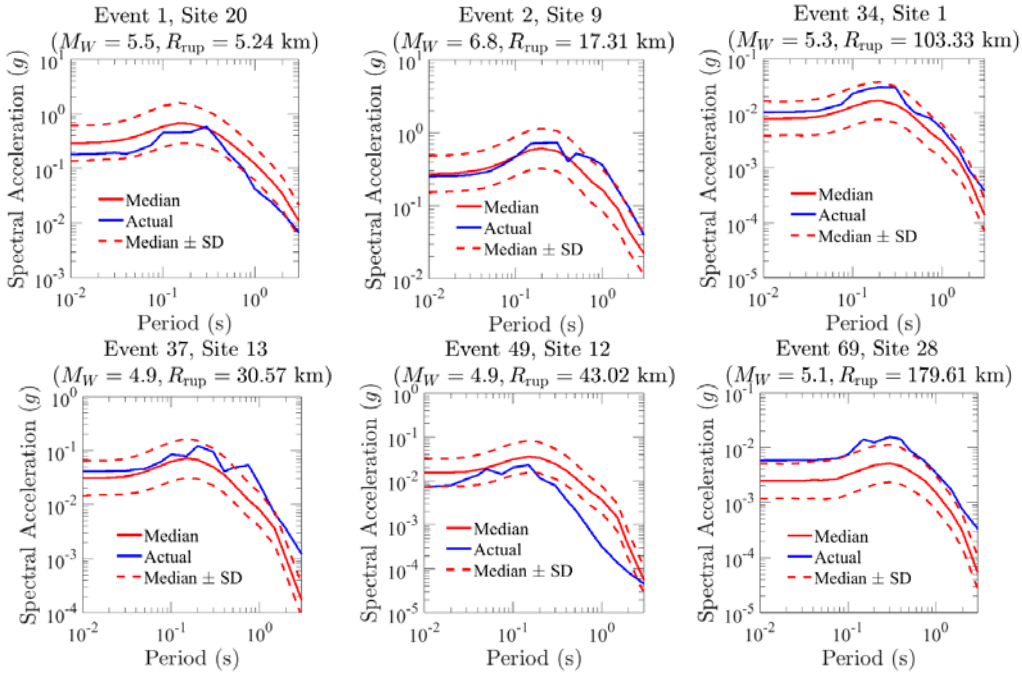

Fig. 11 Comparisons of median and median ± one standard deviation predictions of 5%-damping SA spectrum by the selected GMPE (for shallow crustal earthquakes) with the actual SA spectrum for widely differing event-site combinations (with the corresponding values of M_W and R_{rup} indicated)

The selected GMPE by Abrahamson and Silva [72] predicts the median level of SA (in g) as well as the associated standard deviation SD at 20 natural periods between 0.01 and 10 s in terms of magnitude, distance, site soil condition, and other source and site parameters. Figure 11 shows the comparisons between the "median" and "median ± SD" predictions of 5%-damping SA spectrum from the selected GMPE with the actual 5%-damping (geometric-mean) SA spectrum for several typical examples of widely differing combinations of magnitude, distance, and site conditions. The details of earthquake events and recording sites for the event-site combinations considered in these examples are given in Jaisal [85]. It is observed that the selected GMPE is able to predict the SA values in an overall satisfactory manner.

2. GMPE for Hindukush Subduction Zone Earthquakes

To select a suitable GMPE for the Hindukush subduction zone earthquakes, five GMPEs are shortlisted in the initial selection based on the criteria of Bommer et al. [70]. These equations have been proposed by Atkinson and Boore [89], Gupta [90], Lin and Lee [91], Youngs et al. [92], and Zhao et al. [93]. Table 6 gives the salient features of these equations, including the regions for which those have been developed, their magnitude, distance, and period ranges of applicability, and distance metrics and site classification parameters used in those. All the five candidate equations give the estimates of the logarithm of SA at 5% damping for the horizontal motions.

Table 6: Particulars of candidate GMPEs considered for subduction zone earthquakes

S. No.	Candidate Equation	Host Region	Magnitude Range	Distance Metric	Distance Range (km)	Period Range (s)	Site Classification Parameter
1	Atkinson and Boore [89]	Worldwide	5.0–8.3	R_{rup}	11–550	0.04–3	NEHRP (A, B, C, D, E)
2	Gupta [90]	Northeast India	5.0–8.3	R_{rup}	11–550	0.02–3	NEHRP (A, B, C, D, E)
3	Lin and Lee [91]	Northeast Taiwan & worldwide	4.1–7.3	R_h	40–600	0–5	Qualitative (rock & soil)
4	Youngs et al. [92]	Worldwide	> 5.0	R_{rup} (rock) R_h (soil)	10–500	0–3 (rock) 0–4 (soil)	Qualitative (rock & soil)
5	Zhao et al. [93]	Japan & worldwide	5.0–8.3	R_{rup}	0–300	0–5	NEHRP (A, B, C, D, E)

A total of 19 baseline-corrected strong ground motion records from six Hindukush zone earthquakes (Gupta [84]; Gupta and Trifunac [80]) are considered for the performance evaluation of the five candidate GMPEs. Figure 12 shows the distribution of these records with respect to magnitude M_W and epicentral distance R_e for different ranges of V_{S30} at the recording sites. It may be observed that all the 19 motions have been recorded at the epicentral distances greater than 600 km. For computing various distance metrics involved in the candidate GMPEs, the angle of dip for the Hindukush subduction zone is taken as 70°, and strike is taken to change from eastward to NE around the 71°E longitude based on the distribution of the epicenters of past earthquakes (Pegler and Das [29]; Singh et al. [20]). The subduction earthquakes are considered as in-slab type events due to the depths of all the six events being greater than 50 km (Atkinson and Boore [89]; Lin and Lee [91]). Further, qualitative site characterization in the candidate equations by Lin and Lee [91] and Youngs et al. [92] as rock or soil is carried out based on the NEHRP classes adopted by Mittal et al. [86], and Classes A and B are taken as rock sites and the other classes (C, D, and E) as soil sites.

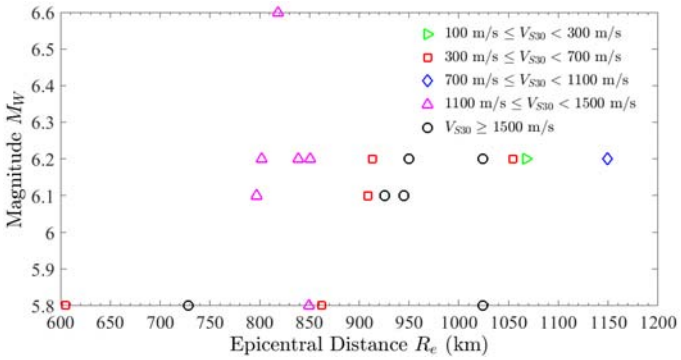

Fig. 12 Distribution of ground motion records for Hindukush subduction earthquakes with respect to magnitude M_W and epicentral distance R_e for different ranges of V_{S30} values at recording sites

For the performance evaluation of the five candidate GMPEs, the 323 estimates of the normalized residuals NR and corresponding LH values are obtained from the geometric-mean SA values of the two horizontal components of the 19 recorded accelerograms computed at 17 natural periods. Those are then used to plot the histograms shown in Figures 13(a)–13(e) for the candidate GMPEs by Atkinson and Boore [89], Gupta [90], Lin and Lee [91], Youngs et al. [92], and Zhao et al. [93], respectively. These figures also show the comparisons of the normal distributions fitted to the NR histograms with the standard normal distribution. Further, the goodness-of-fit measures, i.e., the mean and SD of normalized residuals NR, and the median of LH values, are indicated in each of the figures and listed in Table 7 for the five GMPEs. From these results, with the mean of 0.037 being closest to 0 and the median of 0.636 being closest to 0.5, the GMPE by Lin and Lee [91] is considered to be most appropriate for the present study. Though the SD of 0.771 indicates an underestimation of standard deviation, which is also confirmed by the median greater than 0.5, the mismatch of the standard deviation may be ignored as in the case of the shallow crustal earthquakes.

Table 7: Goodness-of-fit measures for the candidate GMPEs considered for Hindukush subduction zone earthquakes

Serial No.	Candidate GMPE	Mean of NR Values	SD of NR Values	Median of LH Values
1	Atkinson and Boore [89]	6.771	1.464	0.000
2	Gupta [90]	3.702	1.052	0.000
3	Lin and Lee [91]	0.037	0.771	0.636
4	Youngs et al. [92]	0.861	0.696	0.362
5	Zhao et al. [93]	4.886	1.371	0.000

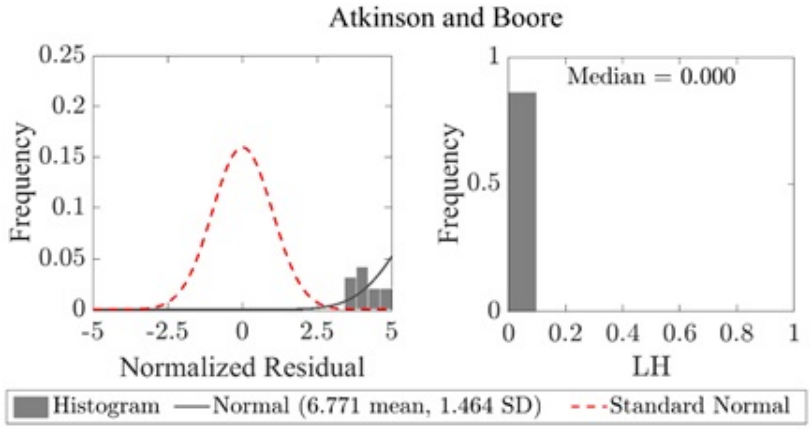

(a)

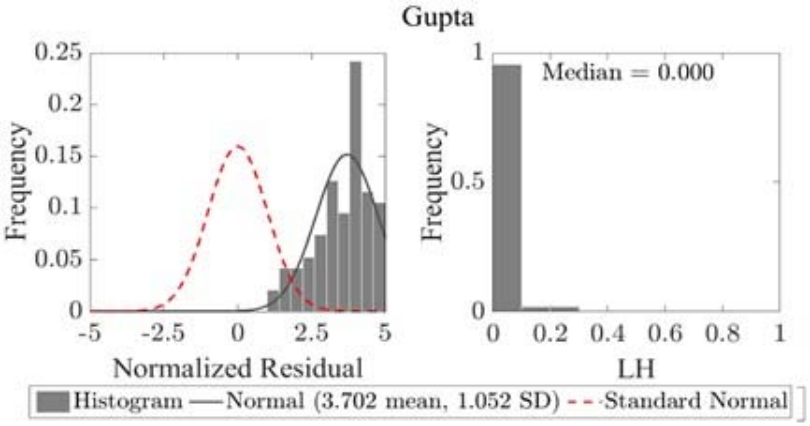
Gupta
Frequency
Normalized Residual
Median = 0.000
LH
Histogram
Normal (3.702 mean, 1.052 SD)
Standard Normal

(b)

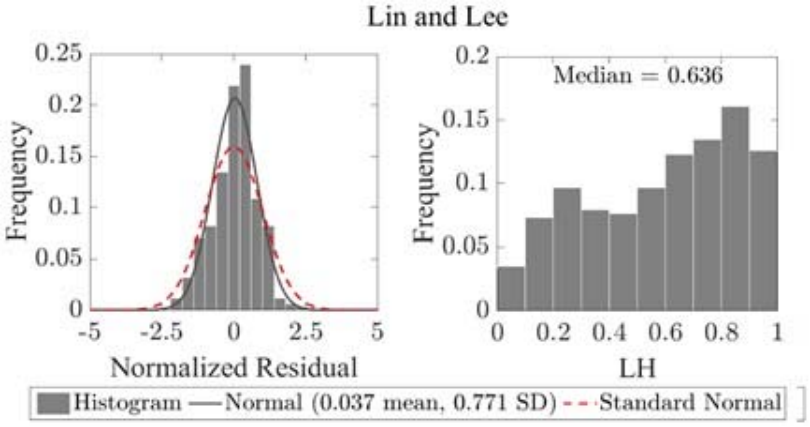
Lin and Lee
Frequency
Normalized Residual
Median = 0.636
LH
Histogram
Normal (0.037 mean, 0.771 SD)
Standard Normal

(c)

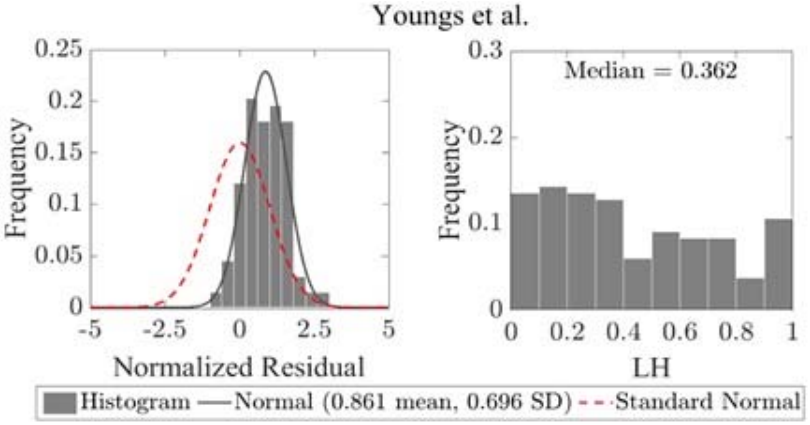
Youngs et al.
Frequency
Normalized Residual
Median = 0.362
LH
Histogram
Normal (0.861 mean, 0.696 SD)
Standard Normal

(d)

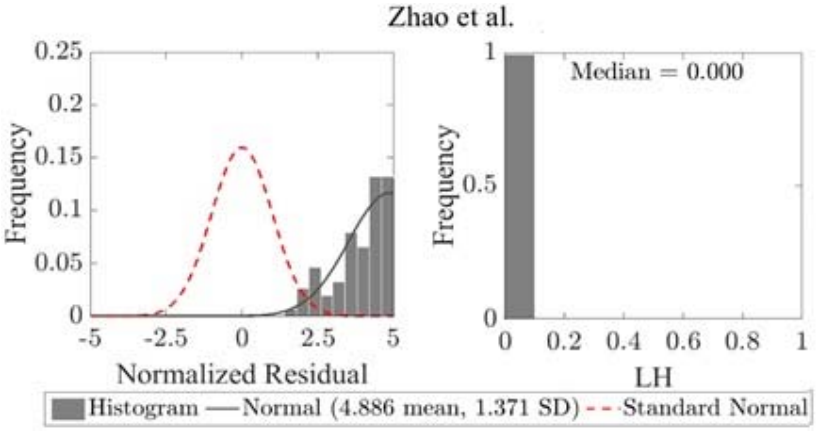

(e)

Fig. 13 (left) Comparison of the histograms of the normalized residuals, NR, and the best-fit normal distributions (solid curves; with the mean and SD values as indicated) with the standard normal distribution (dashed curves), and (right) the histograms of corresponding likelihood function LH values (with the median values indicated), for the candidate GMPEs by (a) Atkinson and Boore [89], (b) Gupta [90], (c) Lin and Lee [91], (d) Youngs et al. [92], and (e) Zhao et al. [93]

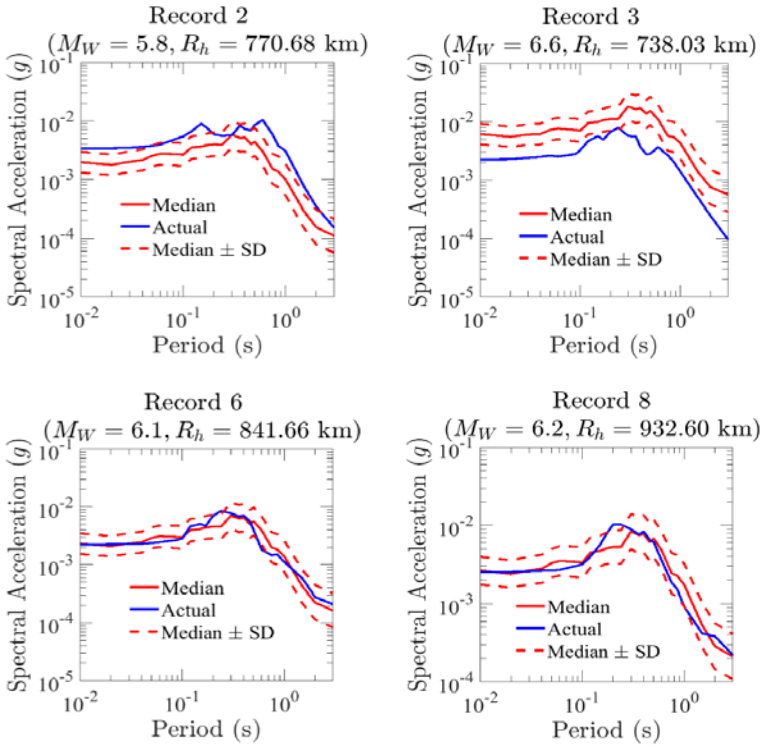

Fig. 14 Comparisons of median and median ± one standard deviation predictions of 5%-damping SA spectrum by the selected GMPE (for Hindukush subduction zone) with the actual SA spectrum for widely differing event-site combinations (with the corresponding values of M_W and R_h indicated)

The selected GMPE by Lin and Lee [91] predicts the median level of SA (in g) as well as the associated standard deviation SD in terms of moment magnitude M_W, hypocentral distance R_h, and focal depth H, for rock and soil site conditions. The regression coefficients and standard deviations are given separately for the rock and soil sites at 27 natural periods between 0.01 and 5 s. For the purpose of

hazard computations in the present study, these values are interpolated on the log-log scale at the same 17 natural periods as considered for the relation of Abrahamson and Silva [72]. Figure 14 shows comparisons between the "median" and "median ± SD" predictions of 5%-damping SA spectrum from the selected GMPE with the actual 5%-damping (geometric-mean) SA spectrum for four typical examples of widely differing combinations of magnitude, distance, and site conditions. The details of earthquake events and recording stations for the records considered in these examples are given in Jaisal [85]. It may be observed from these examples that the SA values predicted by the selected GMPE are in very good agreement with the amplitudes and trends of the SA spectra of the recorded motions.

HAZARD COMPUTATION AND MAPPING

1. Mathematical Formulation and Input Parameters

The zoning maps for the northwestern Himalayan region of India are prepared in terms of the 5%-damping spectral acceleration amplitudes, $\mathrm{SA}(T)$, for different combinations of natural period T and return period T_R. The mathematical formulation used for the computation of hazard can be expressed in the following discrete form (Anderson and Trifunac [94]; Gupta [95])

$$\upsilon[\mathrm{SA}(T)] = \sum_{n=1}^{N}\sum_{j=1}^{J_n}\sum_{i=1}^{I_n} q_n[\mathrm{SA}(T)\,|\,M_j, R_i]\,\lambda_n(M_j, R_i) \tag{5}$$

Here, $\upsilon[\mathrm{SA}(T)]$ is the occurrence rate of spectral amplitudes greater than or equal to $\mathrm{SA}(T)$ at the natural period *T*, $\lambda_n(M_j, R_i)$ is the occurrence rate of earthquakes of magnitude M_j in the *n*th seismic source at the source-to-site distance R_i, and $q_n[\mathrm{SA}(T)\,|\,M_j, R_i]$ is the probability of spectral amplitudes exceeding $\mathrm{SA}(T)$ due to the earthquake magnitude M_j at the distance R_i from the *n*th source, and other governing site and source parameters not mentioned here for brevity. The summations in Equation (5) are performed over the *N* number of sources, and J_n number of magnitudes and I_n number of distances in the *n*th source. The reciprocal of the occurrence rate $\upsilon[\mathrm{SA}(T)]$ obtained from Equation (5) gives the return period T_R (in years) for the spectral amplitude $\mathrm{SA}(T)$. Also, on assuming the earthquake events to follow a Poisson distribution, the probability of spectral amplitudes exceeding $\mathrm{SA}(T)$ during an exposure period Y (in years) can be defined as

$$P(\mathrm{SA}(T)\,|\,Y) = 1 - \exp[-\upsilon(\mathrm{SA}(T))\cdot Y] \tag{6}$$

The zoning maps in this study are prepared for the spectral amplitudes having 29%, 10%, 5%, and 2% probabilities of exceedance in an exposure period of 50 years, which correspond to the return periods of 145, 475, 975, and 2475 years, respectively.

The probability $q_n[\mathrm{SA}(T)\,|\,M_j, R_i]$ in Equation (5) is estimated by using the normal distribution with the mean and standard deviation values of $\ln \mathrm{SA}(T)$ obtained from the applicable GMPE (for the *n*th source) for a set of M_j, R_i, and other governing parameters. The occurrence rate $\lambda_n(M_j, R_i)$ for the *n*th area type source is estimated by using the recurrence relationship of Equation (3) with the parameters listed in Table 3 (and a suitably selected minimum magnitude $M_{\min}$) and obtaining the total occurrence rate $n(M_j)$ in the magnitude bin $(M_j - \delta M_j, M_j + \delta M_j)$ out of nine magnitude bins with central magnitudes M_j = 5.0, 5.4, …, 8.2 and $\delta M_j = 0.2$. The number $n(M_j)$ is then distributed non-uniformly over the grid cells of size 0.1°×0.1° (in latitude and longitude) covering the entire area of the *n*th source, and the occurrence rate $\lambda_n(M_j, R_i)$ is obtained by estimating the desired type of distance metric for each grid cell.

The number $n(M_j)$ is distributed by using a weighted distribution, wherein the weight w_i for the *i*th grid cell is defined by using a circular Gaussian smoothing of the past seismicity as (Gupta [81])

$$w_i = \frac{\bar{n}_i}{\sum_k \bar{n}_k}; \quad \text{with} \quad \bar{n}_i = \frac{\sum_j n_j e^{-\Delta_{ij}^2/c^2}}{\sum_j e^{-\Delta_{ij}^2/c^2}} \tag{7}$$

Here, n_i is the observed number of earthquakes in the *i*th grid cell above $M_{\min}$, Δ_{ij} is the distance between the centers of the *i*th and *j*th grid cells, and c characterizes the uncertainty in the epicentral location and is assumed to be 20 km. The summations over j in Equation (7) are taken by considering all the grid cells lying within 5*c* distance from the *i*th grid cell, and the summation over k is taken by considering all the grid cells in the *n*th source.

The attenuation relation of Abrahamson and Silva [72] selected for the 16 area type sources with shallow crustal earthquakes is defined in terms of the closest distance to the fault rupture plane, R_{rup}. In order to assign this distance for the *i*th grid cell in the source zone under consideration, a fault rupture plane needs to be associated to the magnitude-M_j event assumed to occur at the center of the grid cell. This cannot be done in a unique way for an area type source, and several different ways have therefore been proposed by researchers for this purpose (Petersen et al. [96]; Kaklamanos et al. [97]; Pagani et al. [98]; Campbell and Gupta [99]; etc.). In this study, the methodology proposed by Gupta [81] is adopted, wherein a rectangular fault rupture plane having its geometric centre as the hypocenter at a depth H_j is considered, and R_{rup} is taken as the average of the values calculated for the preferred dip angle given in Table 1 and strike angles distributed uniformly over the range given in Table 1. The length and width of the rupture plane are estimated corresponding to M_j by using the self-consistent relations of Leonard [82]. The hypocentral depths in a source zone are assigned based on a careful study of the focal depths of the past events and geotectonic features of the source zone. These depths for the nine central magnitudes considered in the case of the 16 area type sources are given in Table 8. It may be observed that larger-magnitude events are in general characterized by larger focal depths.

Table 8: Assigned focal depths to different central magnitudes of earthquakes for the 16 area type source zones

Source No.	Name of Source Zone	Focal Depths, H_j (in km), for Different Central Magnitudes, M_j								
1–2	Pamir-Tian Shan block; Tarim basin	M_j	5.0	5.4	5.8	6.2	6.6	7.0	7.4	7.8	8.2
		H_j	20	20	20	20	20	20	20	20	20
4–9	Karakoram area; Kunlun and western Tibet area; Kohistan-Nanga Parbat area; Ladakh block; Lhasa block; Himalayan syntaxial zone	M_j	5.0	5.4	5.8	6.2	6.6	7.0	7.4	7.8	8.2
		H_j	10	14	18	22	26	30	30	30	30
10–13	Western Himalayas-I; Western Himalayas-II; Western Himalayas-III; Western Nepal Himalayas	M_j	5.0	5.4	5.8	6.2	6.6	7.0	7.4	7.8	8.2
		H_j	10	12	14	16	18	20	20	20	20
14–17	Western plate boundary; Salt range area; Delhi-Hardwar ridge; Indo-Gangetic plain	M_j	5.0	5.4	5.8	6.2	6.6	7.0	7.4	7.8	8.2
		H_j	10	11	12	13	14	15	15	15	15

The attenuation relation of Lin and Lee [91] selected for the Hindukush subduction source (shown as Source 3 in Figure 6) uses the hypocentral distance R_h and focal depth H as input distance parameters. This source zone is represented by a curved fault plane dipping steeply at an angle of 70°. The dip direction is to the north for the segment trending in the west-east direction between 69.2°E and 70.8°E, and to the northwest for the segment trending SW-NE further up to about 72°E. Based on the focal depths of past earthquakes, the top edge of the fault plane is taken at a depth of 50 km. The non-uniform spatial distribution of seismicity for this source is modeled by a weighted distribution of the occurrence rates $n(M_j)$ over the 0.1°×0.1° size grid cells covering the surface projection of the fault plane as for the area sources, while considering only six magnitude bins with central magnitudes $M_j = 5.8, 6.2, \cdots, 7.8$ and $\delta M_j = 0.2$. Further, the hypocentral distance R_h for the *i*th grid cell is obtained by taking focal depth as the depth to the fault plane vertically below the center of the grid cell. The weighted occurrence rates along with the distances thus obtained define the rates, $\lambda_n(M_j, R_i)$, for Source 3 in Equation (5).

The calculation of $\upsilon[\mathrm{SA}(T)]$ in Equation (5) is carried out at a site by considering the grid cells within a radius of 300 km of the site and a maximum of 75 intervals of distances to these cells. These intervals are defined as $(R_i - \delta R_i, R_i + \delta R_i)$ with δR_i taken as 1 km for R_i up to 30 km, 2 km for R_i between 30 and 50 km, 5 km for R_i between 50 and 150 km, and 10 km for R_i between 150 and 300 km, such that these intervals are almost equally sized on the logarithmic scale. The occurrence rate $\lambda_n(M_j, R_i)$ for the *i*th distance interval is taken as the total of the occurrence rates (in the magnitude bin $(M_j - \delta M_j, M_j + \delta M_j)$) for all the grid-cell centers of the *n*th source falling in the interval $(R_i - \delta R_i, R_i + \delta R_i)$. The hanging wall effects in the GMPE of Abrahamson and Silva [72] are modeled by defining the additional parameters like the dip angle of fault plane δ, depth to the upper edge of the fault rupture Z_{tor}, perpendicular distance from the site to the surface projection of the upper edge of the fault rupture R_x, and the closest distance to the surface projection of fault rupture R_{jb}, by using somewhat conservative approximations of thrust faulting with fixed values of dip angle as 40° and source-to-site azimuth as 90°.

2. Hazard Mapping

The hazard computations are carried out (by using a FORTRAN program developed by the second author) at 807 locations with 0.2°×0.2° (in latitude and longitude) spacing, while assuming rock type site conditions with V_{S30} = 1500 m/s. For each of the five return periods considered, hazard maps are prepared for five natural periods of 0.01, 0.1, 0.2, 1, and 3 s as given in Jaisal [85]. The maps for the period of 0.01 s are considered to represent the maps for PGA. Further, the maps for the return periods of 475 and 2475 years are considered to represent the hazard values for the design basis event (DBE) and maximum considered event (MCE) in accordance with the codal provisions (ICC [100]; ASCE [101]). Figures 15(a)–15(e) show the maps for PGA and the natural periods of 0.1, 0.2, 1.0, and 3.0 s, respectively, with the DBE maps shown on the left and MCE maps on the right.

The spatial distribution of hazard in the maps of Figures 15(a)–15(e) is seen to vary significantly with both natural period and return period. The maps for shorter natural periods are characterized by large local peaks as compared to those for the longer periods. This is because the short-period hazard is dominated by the local earthquakes of smaller magnitudes, whereas the long-period hazard has significant contributions from larger magnitudes at all the distances considered. The long-period hazard is thus characterized by smoother site-to-site variations compared to the short-period hazard with dominant contributions only from the nearby sources. With an increase in the return period, the hazard level increases in general, but the pattern of spatial distribution for a given natural period is not seen to vary much.

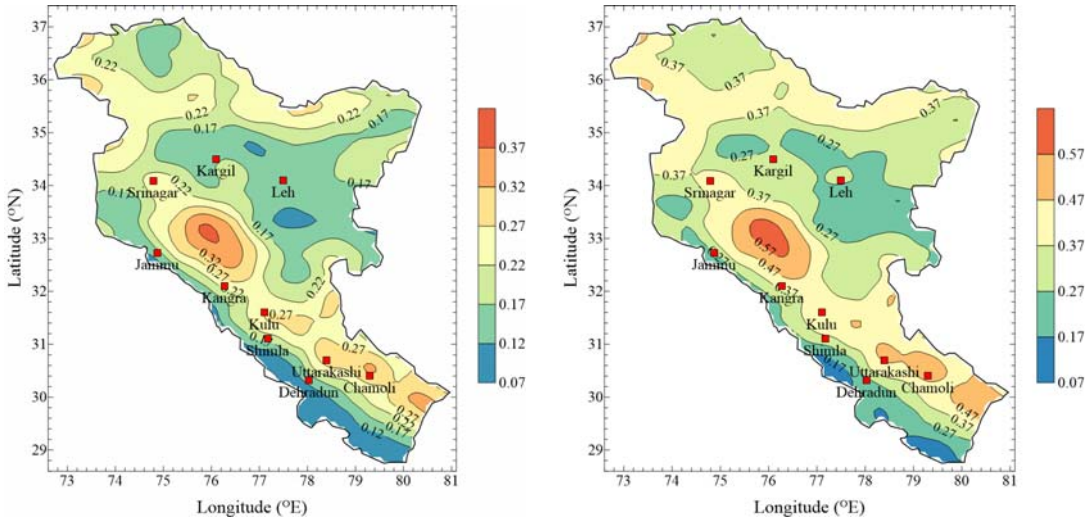
Latitude (°N)
Longitude (°E)
Kargil
Leh
Srinagar
Jammu
Kangra
Kulu
Shimla
Uttarakashi
Dehradun
Chamoli
0.37
0.32
0.27
0.22
0.17
0.12
0.07
0.57
0.47
0.37
0.27
0.17
0.07

(a)

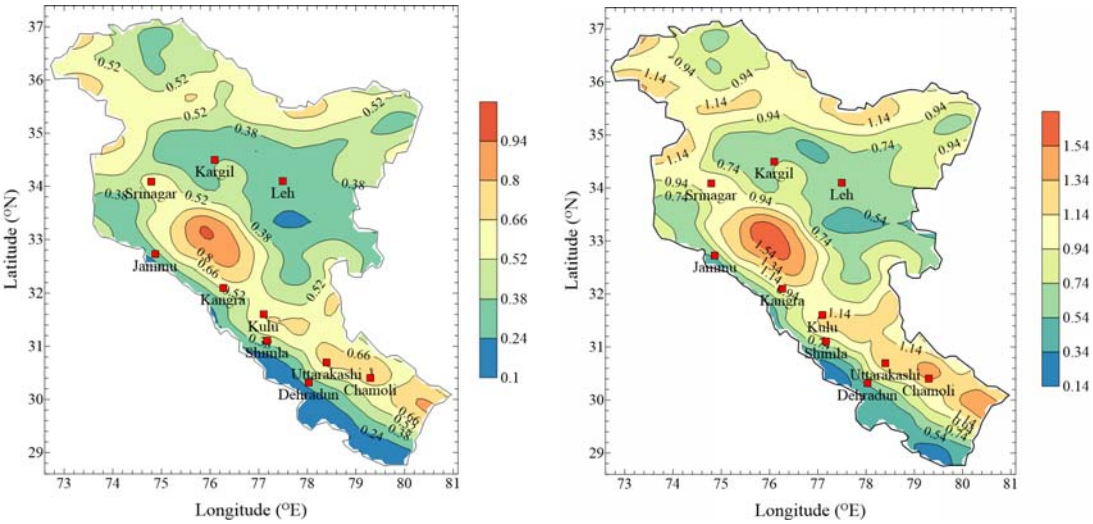
Latitude (°N)
Longitude (°E)
Kargil
Leh
Srinagar
Jammu
Kangra
Kulu
Shimla
Uttarakashi
Dehradun
Chamoli
0.94
0.8
0.66
0.52
0.38
0.24
0.1
1.54
1.34
1.14
0.94
0.74
0.54
0.34
0.14

(b)

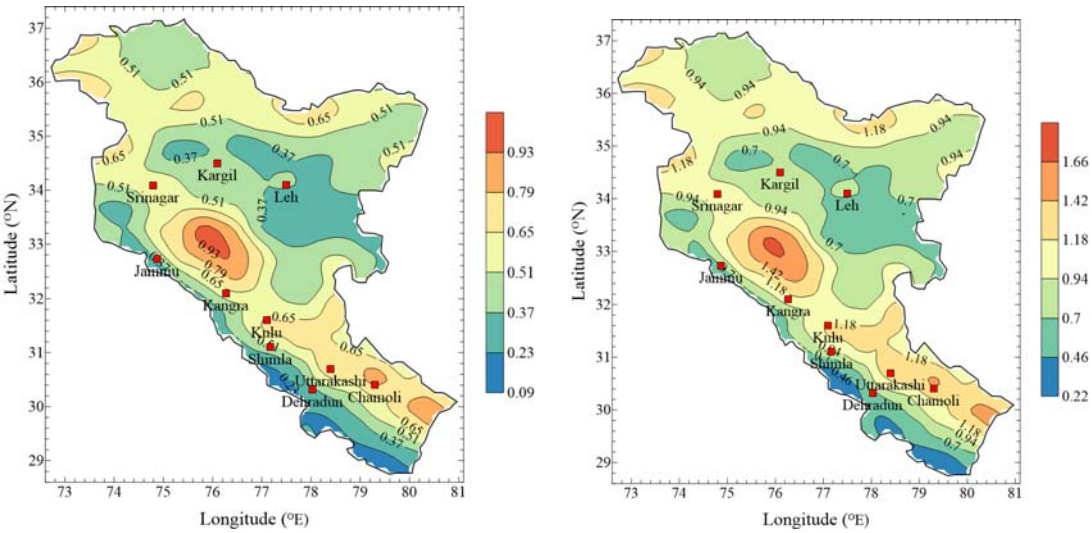
Latitude (°N)
Longitude (°E)
Kargil
Leh
Srinagar
Jammu
Kangra
Kulu
Shimla
Uttarakashi
Dehradun
Chamoli
0.93
0.79
0.65
0.51
0.37
0.23
0.09
1.66
1.42
1.18
0.94
0.7
0.46
0.22

(c)

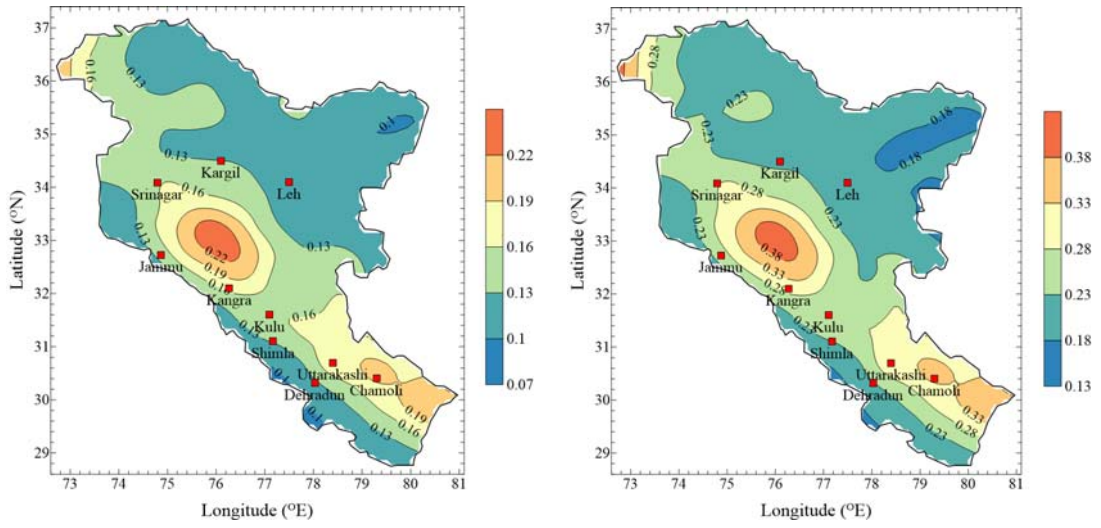

(d)

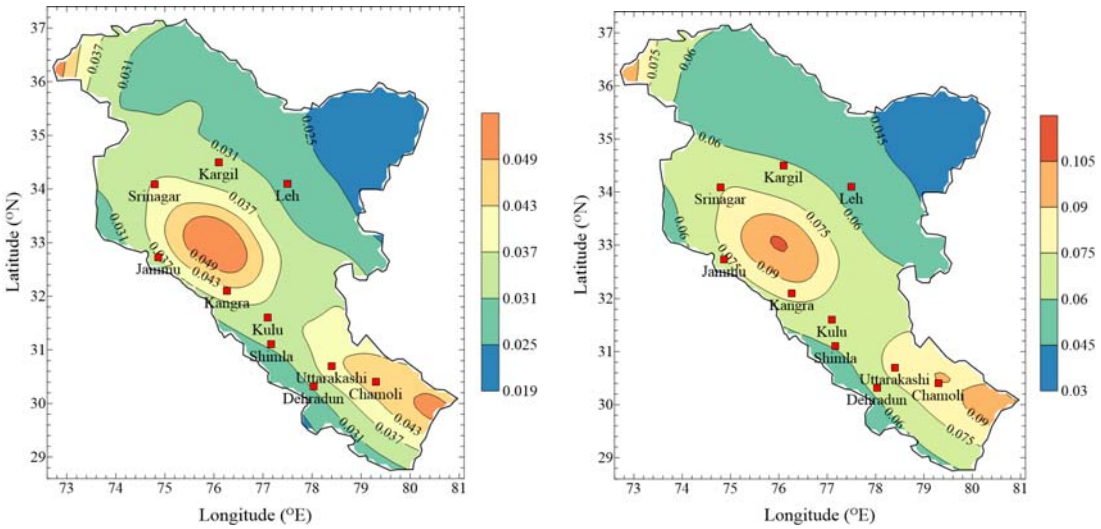

(e)

Fig. 15 Hazard maps for the return periods of 475 years (left) and 2475 years (right) in terms of (a) PGA, and SA(T) for 5% damping ratio and natural periods of (b) 0.1 s, (c) 0.2 s, (d) 1.0 s, and (e) 3.0 s

The hazard maps indicate that the most vulnerable sites in the northwest Himalayan region lie along the Himalayan thrust belt. Regardless of the natural period and return period, the contours are consistently seen peaking in the zone enclosing the MBT and MCT faults. For example, in the vicinity of Kishtwar around 33.3°N and 75.7°E in this zone, the MCE-level PGA and SAs at 0.2 and 1.0 s periods become as high as $0.62\,g$, $1.78\,g$, and $0.42\,g$, respectively. The area of Chamoli, which has witnessed several destructive earthquakes in the past, corresponds to the maximum PGA of $0.54\,g$ and the maximum SAs of $1.58\,g$ and $0.34\,g$ at 0.2 and 1.0 s periods, respectively (at the MCE level). The high levels of hazard in this area are due to the high seismic potential. Further, the faster decay of hazard on either side of this area at shorter periods is due to the abundance of small earthquakes, which generate short-period seismic waves.

High hazard levels are also seen in the Kohistan-Nanga Parbat and Karakoram areas, where the MCE-level estimates of PGA and SAs at 0.2 and 1.0 s periods are $0.46\,g$, $1.38\,g$, and $0.38\,g$, respectively. In addition to the fact that these areas are in a highly unstable tectonic setting with major features, such as the main Karakorum thrust, main mantle thrust, Karakoram and Karakax faults, the intense seismic activity in Hindukush and Pamirs may also be responsible for these hazard levels. On the

other hand, lower hazard levels are observed in the Ladakh block, and, as expected, the areas to the south of MBT are characterized by the lowest hazard levels.

HAZARD MAPS BASED ON UNIFORM DISTRIBUTION OF SEISMICITY

Several studies in the past (see, for example, Kanagarathinam et al. [102]; Revathi and Pandurangan [103]; Sitharam and Kolathayar [104]; Rout et al. [11]) have assumed the uniform spatial distribution of seismicity within each seismic source in their PSHA calculations. This assumption is found to lead to very unrealistic hazard maps in this study. For example, the DBE and MCE levels of PGA and SAs at 0.2 s and 1.0 s periods shown in Figures 15(a), 15(c), and 15(d) are modified to the levels shown in Figures 16(a), 16(b), and 16(c), respectively. It may be observed that with the peaks and valleys of contours disappearing, the uniform spatial distribution of seismicity leads to a diffused spatial distribution of hazard. Due to this, the site-specific hazard characterization gets replaced by a spatially-uniform hazard characterization over larger areas, which may underestimate or overestimate the hazard at specific sites, depending upon whether a site is located in a high or low seismic potential zone. For example, the assumption of uniform seismicity distribution results in an underestimation of hazard in the highly vulnerable cities like Chamoli, Srinagar, and Uttarakashi, while hazard in the cities like Dehradun and Jammu with lesser vulnerability is overestimated.

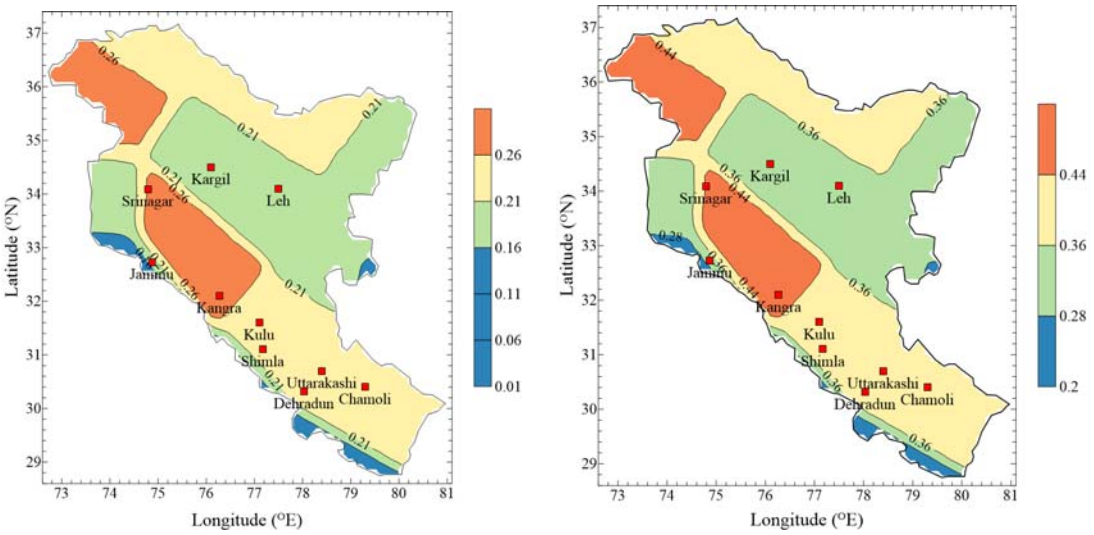

(a)

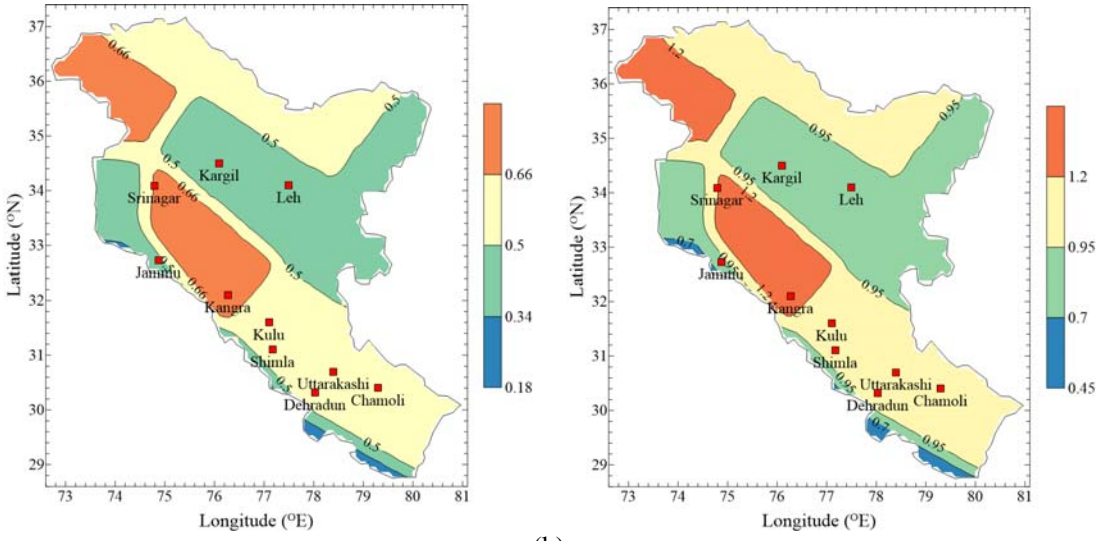

(b)

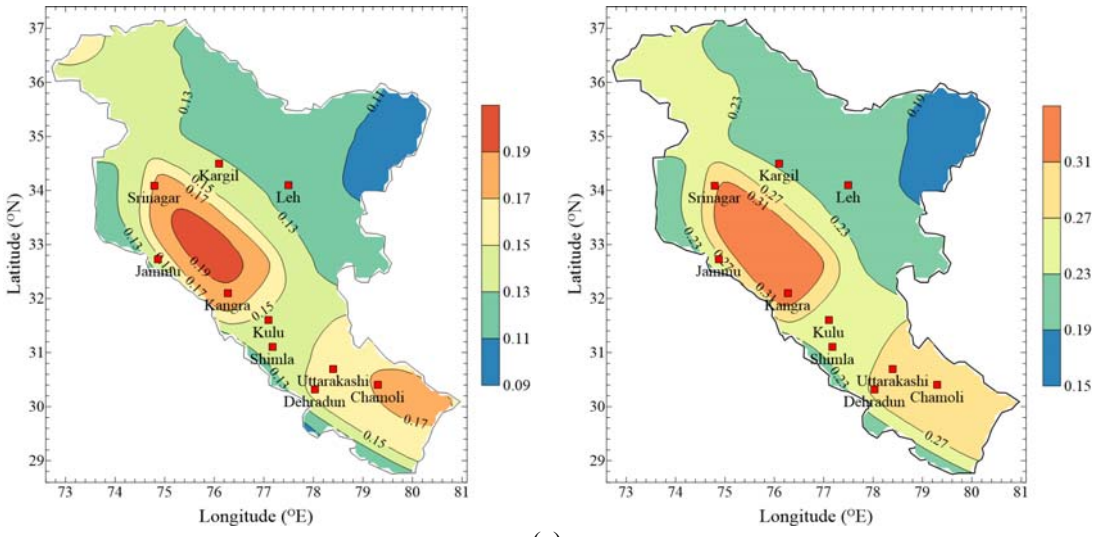

(c)

Fig. 16 Hazard maps based on the uniform distribution of seismicity for the return periods of 475 years (left) and 2475 years (right) in terms of (a) PGA, and SA(*T*) for 5% damping ratio and natural periods of (b) 0.2 s, and (c) 1.0 s

COMPARISON WITH OTHER STUDIES

Seismic hazard assessment studies for a part or whole of the study region have been carried out in the past by Khattri et al. [3], Bhatia et al. [4], Parvez et al. [5], NDMA [105], and Nath and Thingbaijam [8]. Table 9 shows a comparison of the DBE-level PGA estimates from these studies for the 10 selected cities of Chamoli, Dehradun, Jammu, Kangra, Kargil, Kulu, Leh, Shimla, Srinagar (Jammu & Kashmir), and Uttarakashi with the results of this study. It may be observed that the estimates of Nath and Thingbaijam [8] are much higher compared to those by the other five studies, except in the case of the estimate for Kangra by Khattri et al. [3]. Further, the estimates given by Khattri et al. [3], Bhatia et al. [4], and Parvez et al. [5] do not show the required site-specific variations among different cities. The estimates of NDMA [105] and Nath and Thingbaijam [8] show much wider variations, but with significantly different trends and amplitudes.

Table 9: Comparison of the DBE-level PGA estimates (in *g*) from the present study with five previous studies at 10 selected cities spread over the entire region of study

Serial No.	City	Khattri et al. [3]	Bhatia et al. [4]	Parvez et al. [5]	NDMA [105]	Nath and Thingbaijam [8]	Present Study
1	Chamoli	0.30	0.28	0.23	0.14	0.53	0.31
2	Dehradun	0.30	0.23	0.06	0.08	0.47	0.14
3	Jammu	0.30	0.13	0.23	0.08	0.33	0.16
4	Kangra	0.70	0.28	0.23	0.11	0.37	0.24
5	Kargil	0.05	0.08	0.06	0.10	0.23	0.19
6	Kulu	0.30	0.28	0.06	0.12	0.40	0.29
7	Leh	0.05	0.13	0.06	0.07	0.18	0.09
8	Shimla	0.30	0.23	0.06	0.13	0.42	0.19
9	Srinagar	0.30	0.23	0.23	0.08	0.33	0.24
10	Uttarakashi	0.30	0.28	0.23	0.11	0.53	0.29

Large differences observed in the hazard estimates of different studies may largely be related to the differences in the methodology adopted, assumptions or idealizations made in defining the seismicity, attenuation relation used, and to the quality and size of the database available at the time of study. The studies by Khattri et al. [3] and Bhatia et al. [4], which are similar in their approaches in respect of the delineation and characterization of sources, consider very large areal seismic sources, and thus poorly

capture the variations in the seismotectonics of the region. Further, Khattri et al. [3] assumed the attenuation relation by Algermissen and Perkins [106] (developed for eastern United States) based on the similarity of the attenuation of Modified Marcalli intensity (MMI) with distance. Bhatia et al. [4] used the attenuation relation by Joyner and Boore [107] without any apparent justification. The study by Parvez et al. [5] is significantly different from these two studies, as it has followed a deterministic approach based on the computation of synthetic seismograms (Costa et al. [6]).

Among the later studies, NDMA [105] considered large-size area sources for the estimation of a and b values in the G-R relationship. However, this study distributed the occurrence rates for different magnitudes of earthquakes along the known faults and major lineaments in each source, irrespective of the actual distribution of the epicenters of past earthquakes. In addition to the faulty spatial distribution, the seismicity estimated in this study is much lower than that estimated in the present study. Further, the attenuation relations used by NDMA [105] were developed by using the ground motions simulated from the source model approach (Boore [7]), wherein the input parameters used for the simulations were gathered from widely differing studies without mutual consistency and compatibility, and those GMPEs were not validated adequately due to the lack of recorded strong motion data. The predictions of these GMPEs are significantly less than those by the relation of Abrahamson and Silva [72] used in the present study. These factors are primarily responsible for the generally lower hazard estimates of NDMA [105].

Nath and Thingbaijam [8] employed the logic tree approach to consider the epistemic uncertainties in modelling various inputs to the PSHA computations and used the weighted average hazard for preparing the zoning maps. They used eight GMPEs for the shallow crustal earthquakes and four GMPEs for the subduction zone earthquakes with equal weights. Two of these relations, by Campbell and Bozorgnia [73] and Sharma et al. [76], have been found to significantly overestimate the SA amplitudes of recorded motions in the present study. This may partly be responsible for the higher PGA estimates by Nath and Thingbaijam [8]. Other reasons for the higher estimates may be related to the modeling of seismicity and distribution of events in different bins of focal depths. Since Nath and Thingbaijam [8] have not provided any details on these aspects, it is not possible to assess their effects on the hazard levels. Due to the use of non-uniform spatial distribution of seismicity in accordance with the past seismicity, and best GMPEs selected on the basis of recorded strong motion data in the study region, the hazard maps of the present study can be considered as an important update of the maps of the previous studies.

COMPARISON WITH ZONING MAPS OF IS 1893-1 CODE

The BIS code (BIS [1]) demarcates the entire country into four seismic zones, i.e., Zone II, Zone III, Zone IV, and Zone V, with each zone characterized by a zone factor corresponding to the MCE-level PGA. The northwestern Himalayan region of India under study here falls under Zones IV (of severe seismic intensity) and V (of very severe seismic intensity) with the MCE-level PGAs of $0.24g$ and $0.36g$, respectively. Figure 17 shows a comparison of the code-specified zoning map (BIS [1]) with the MCE-level PGA hazard maps (for the return period of 2475 years) obtained for the non-uniform (shown on the left) and uniform (shown on the right) spatial distributions of seismicity in this study. The hatched portions in each map correspond to Zone V of the code-specified map and the remaining region to Zone IV. It may be observed that, with the exception of a very narrow belt along the Himalayan foothills and some portions in the Ladakh region, the non-uniform distribution of seismicity leads to PGAs greater than the code-specified value of $0.24\,g$ (or even $0.36\,g$ in some portions). The uniform spatial distribution is also associated with PGAs significantly higher than the code-specified values in most of the Zone-IV areas. Thus, the zoning map in the BIS code (BIS [1]) for the study region may need to be revised by upgrading some of the regions from Zone IV to Zone V and by specifying Zone VI for the areas with PGA estimates significantly greater than $0.36\,g$.

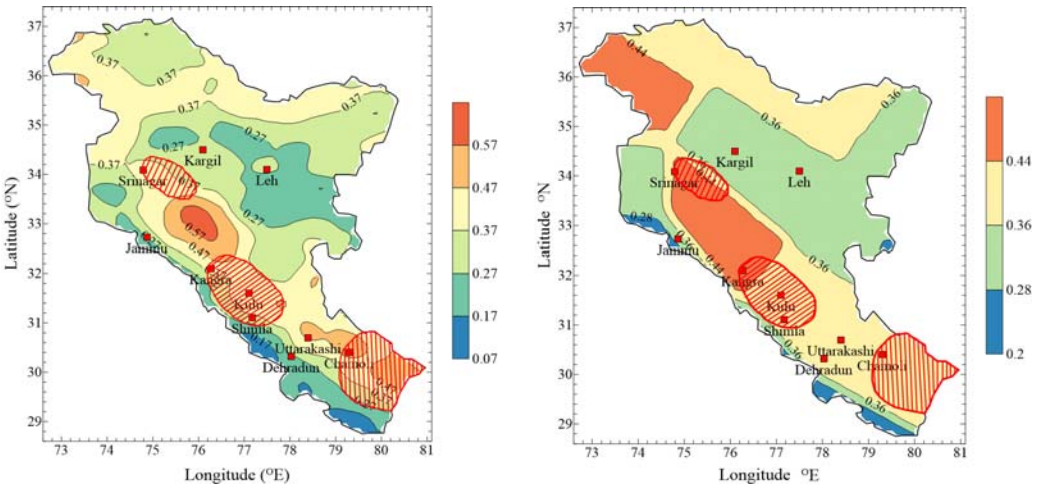

Fig. 17 Comparison of the zoning map of BIS code with the hazard maps for MCE-level PGA (in g) obtained in the present study by using the (left) non-uniform and (right) uniform spatial distributions of seismicity (the hatched portions represent Zone V and the rest of the region Zone IV in the code)

The BIS code (BIS [1]) also gives a standard spectral shape for the damping ratio of 5% and Type I (i.e., rock or hard soil) sites, which can be multiplied with the relevant zone factor to obtain the MCE-level design spectrum at a given site. The BIS spectra thus obtained for the 10 selected cities (see Table 9) are compared in Figures 18(a)–18(j) with the design spectra based on the provisions of the ASCE/SEI 7 standard (ASCE [101]). The PGA values required for the BIS spectra and the SA values at 0.2 and 1.0 s periods required for the ASCE spectra are taken from the MCE-level zoning maps given in Figures 15(a), 15(c), and 15(d), respectively. Figures 18(a)–18(j) show that the BIS spectra match the ASCE spectra well at the intermediate to long periods (say, > 0.5 s), but grossly underestimate the ASCE spectra at the lower periods except in the case of Dehradun (see Figure 18(b)). In view of this, the BIS code (BIS [1]) may be revised by (i) revising the existing zoning map (for the MCE-level PGA) in accordance with Figure 15(a), (ii) introducing an additional zoning map for $\mathrm{SA}_{0.2}$ (i.e., the MCE-level SA at 0.2 s period) similar to that shown in Figure 15(c), and by (iii) replacing the existing expression for the Type I spectral shape by

$$\frac{S_a}{g} = \begin{cases} 1.0 + 10(\mathrm{SA}_{0.2} / \mathrm{PGA} - 1)T; & 0 \le T \le 0.1\,\mathrm{s} \\ \mathrm{SA}_{0.2} / \mathrm{PGA}; & 0.1\,\mathrm{s} \le T \le 0.4\,\mathrm{s} \\ 0.4 \times \mathrm{SA}_{0.2} / (\mathrm{PGA} \times T); & 0.4\,\mathrm{s} \le T \le 4.0\,\mathrm{s} \end{cases} \tag{8}$$

The design spectra based on this expression are also shown in Figures 18(a)–18(j) for the purpose of illustration. It may be observed that the proposed modification would lead to more realistic design spectrum values at the lower periods and somewhat conservative values at the intermediate to long periods.

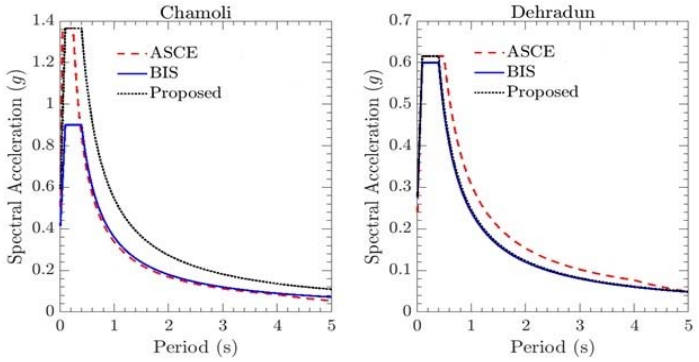

(a) (b)

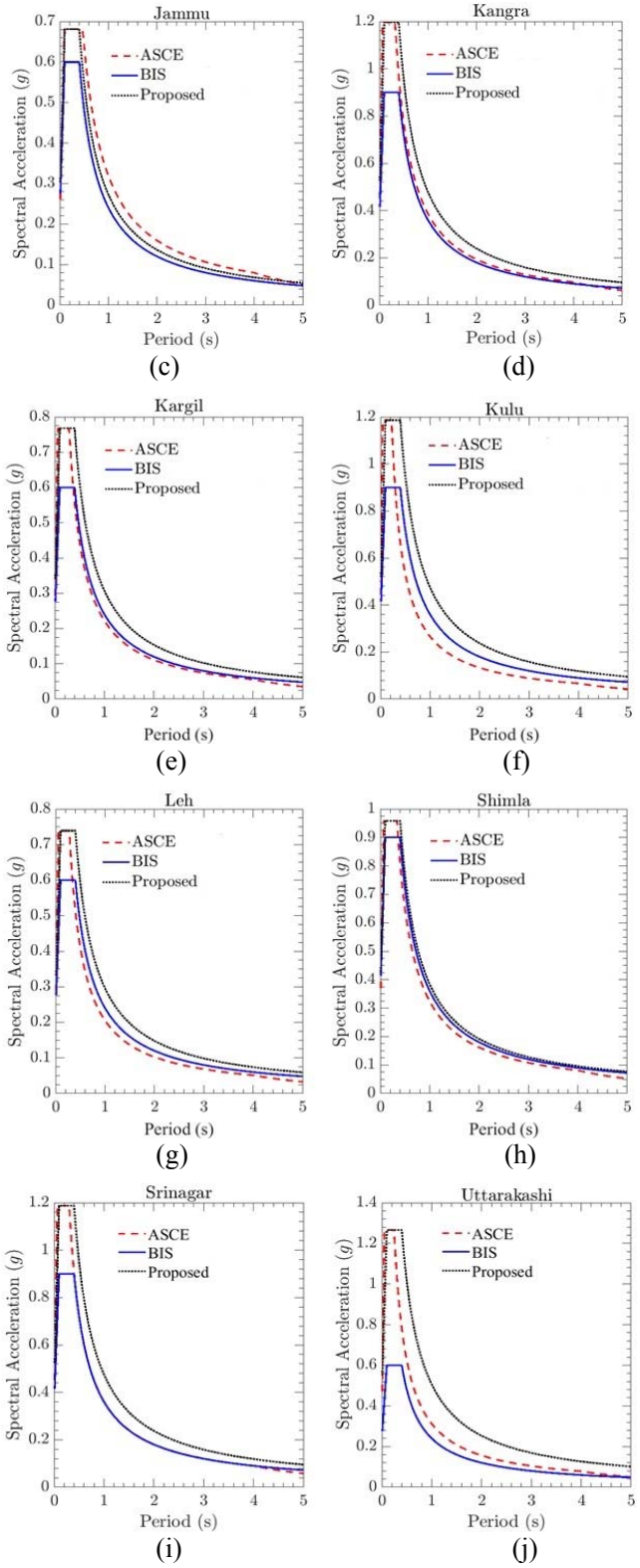

Fig. 18 Comparison of the MCE-level design spectra for rock conditions based on the ASCE [101] and BIS [1] provisions and the proposed revision in BIS [1] provisions for the sites at (a) Chamoli, (b) Dehradun, (c) Jammu, (d) Kangra, (e) Kargil, (f) Kulu, (g) Leh, (h) Shimla, (i) Srinagar, and (j) Uttarakashi

AMPLIFICATION FACTORS FOR OTHER SOIL CONDITIONS

The hazard maps presented in this study can be used to obtain the uniform hazard response spectra for the hard rock site conditions associated with V_{S30} of 1500 m/s or more. For generating uniform hazard spectra for the other site conditions of interest (with V_{S30} < 1500 m/s), an empirical expression is developed here for period-dependent amplification factors, which can be multiplied with the spectra obtained from the hazard maps for the hard rock conditions to give the desired spectra. It is convenient to estimate such amplification factors for given magnitude and distance values directly from the attenuation relations used in the PSHA of the study region, even though the actual amplification factors may be very different from those due to the dependence of probabilistic hazard on multiple sources and multiple magnitude and distance bins (Goulet and Stewart [108]), and hazard maps should ideally be prepared for various values of V_{S30}.

In order to develop an empirical expression for the amplification factors, the actual site amplification factors, AF(T), are obtained based on the PSHA results together with the approximate amplification factors, $\widehat{\text{AF}}(T)$, directly from the GMPE of Abrahamson and Silva [72] at 19 natural periods (from 0.01 to 5 s) for 250 cases comprising 10 sites distributed over the entire study region, five V_{S30} values (of 300, 500, 700, 1100, and 1500 m/s), and five return periods (of 50, 145, 475, 975, and 2475 years). Whereas the actual amplification factor AF(T) for each case is calculated as the ratio of the SA(T) values obtained by the PSHA computations for the desired V_{S30} value and for V_{S30} = 1500 m/s, the approximate amplification factor $\widehat{\text{AF}}(T)$ is obtained as

$$\widehat{\text{AF}}(T) = \exp\left[f_5\left(\text{PGA}_{1100}, V_{S30}\right) - f_5\left(\text{PGA}_{1100}, 1500\right)\right] \tag{9}$$

Here, $f_5(.)$ is the site-response term in the GMPE of Abrahamson and Silva [72], and PGA_{1100} is the PSHA estimate of PGA for V_{S30} = 1100 m/s. The latter is taken here to correspond to the PSHA estimate for the probability of exceedance of 50% in 50 years (i.e., the return period of 72 years) as given in the zoning map of Figure 19.

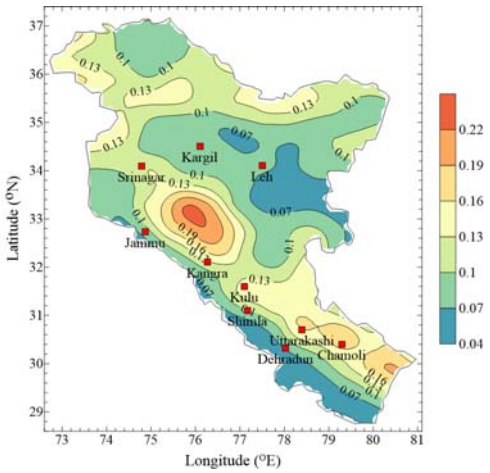

Fig. 19 Hazard map for PGA (in g) in the case of V_{S30} = 1100 m/s and 50% probability of exceedance in 50-year exposure period for the estimation of PGA_{1100}

Figures 20(a)–20(f) show six typical examples of the comparisons between the exact and approximate amplification factors, AF(T) and $\widehat{\text{AF}}(T)$. The cases considered are (a) site location: (36.7° N, 74.9° E), V_{S30} = 300 m/s, return period = 145 years, (b) site location: (35.3° N, 79.3° E), V_{S30} = 500 m/s, return period = 475 years, (c) site location: (33.3° N, 76.5° E), V_{S30} = 700 m/s, return period = 975 years, (d) site location: (32.1° N, 75.9° E), V_{S30} = 300 m/s, return period = 145 years, (e) site location: (34.7° N, 76.5° E), V_{S30} = 500 m/s, return period = 475 years, and (f) site location: (33.9° N, 74.3° E), V_{S30} = 700 m/s, return period = 2475 years. It may be observed that the GMPE-based amplification factors, $\widehat{\text{AF}}(T)$, are consistently lower than the PSHA-based amplification factors, AF(T),

particularly for the cases where nonlinear soil effects are more prominent (i.e., for the periods shorter than ~0.5 s and V_{S30} < 700 m/s). A period-dependent modification factor MF(T) is therefore explored, which is a function of return period and V_{S30} value and can be multiplied with $\widehat{\text{AF}}(T)$ to correct for such differences.

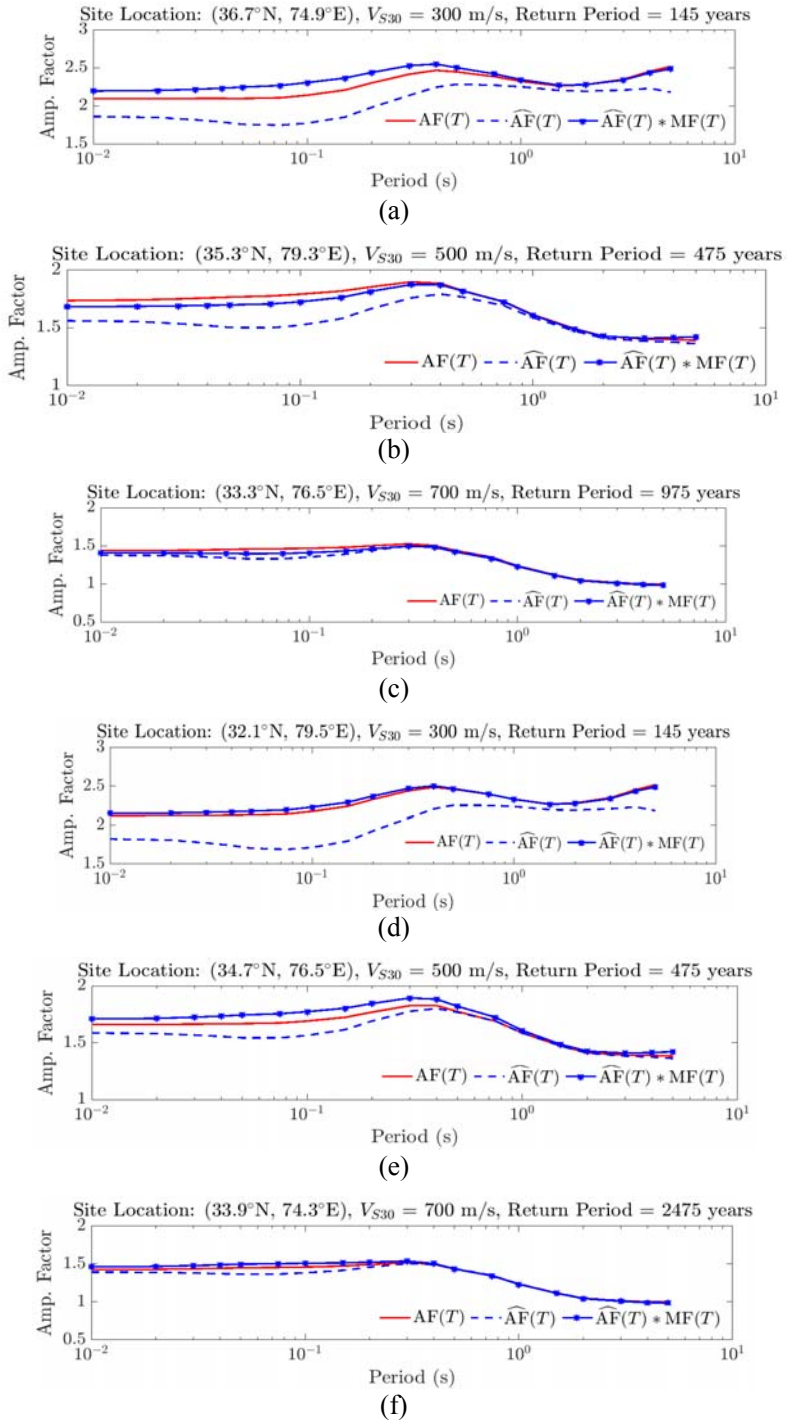

Fig. 20 Comparisons of site amplification factors AF(T), $\widehat{\text{AF}}(T)$, and $\widehat{\text{AF}}(T) * \text{MF}(T)$ for the sites located at (a) (36.7ºN, 74.9ºE), (b) (35.3ºN, 79.3ºE), (c) (33.3ºN, 76.5ºE), (d) (32.1ºN, 75.9ºE), (e) (34.7ºN, 76.5ºE), and (f) (33.9ºN, 74.3ºE) coordinates (with the considered values of V_{S30} and return period indicated)

The 250 sets of AF(T) and $\widehat{\text{AF}}(T)$ curves are used to obtain the modification factors, MF(T) = AF(T)/ $\widehat{\text{AF}}(T)$, at the 19 periods for each set, and then several regression models are attempted to express MF(T) in terms of return period and V_{S30}. Since the regression coefficients associated with return period are consistently found to be negligibly small, the following model is finalized considering V_{S30} as the only parameter:

$$\text{MF}(T) = \exp\left[b_1(T) + b_2(T)\ln V_{S30}\right] \tag{10}$$

Here, $b_1(T)$ and $b_2(T)$ are the (period-dependent) regression coefficients. The values of these coefficients, as obtained from the regression analysis of 250 data points on MF(T) for each period, are given in Table 10. The modified site amplification factors obtained by the multiplication of $\widehat{\text{AF}}(T)$ with MF(T) are also plotted in Figures 20(a)–20(f) for the six example cases. It is seen that the modified estimates of site amplification factors are either on the conservative side or very close to the actual site amplification factors. Similar observations are made in the remaining cases also. Thus, it is proposed to determine the site amplification factors for the hazard estimates obtained in this study by multiplying $\widehat{\text{AF}}(T)$ (see Equation (9)) with MF(T) (see Equation (10)), where the values of PGA_{1100} (in g) to be used in Equation (9) are taken from the map given in Figure 19.

Table 10: Regression coefficients $b_1(T)$ and $b_2(T)$ obtained from regression analysis for the MF(T) model of Equation (10)

Serial No.	Period T (s)	$b_1(T)$	$b_2(T)$
1	0.01 (for zero period)	1.24	−0.19
2	0.02	1.27	−0.19
3	0.03	1.40	−0.21
4	0.04	1.58	−0.24
5	0.05	1.72	−0.26
6	0.075	1.93	−0.29
7	0.1	2.01	−0.30
8	0.15	2.00	−0.30
9	0.2	1.89	−0.29
10	0.3	1.42	−0.22
11	0.4	1.04	−0.16
12	0.5	0.78	−0.12
13	0.75	0.45	−0.07
14	1	0.31	−0.05
15	1.5	0.15	−0.02
16	2	0.04	−0.01
17	3	0.38	−0.06
18	4	0.75	−0.12
19	5	1.13	−0.18

SUMMARY AND CONCLUSIONS

A probabilistic seismic hazard analysis has been performed for preparing the hazard maps of the northwest Himalayan region of India in terms of 5%-damping spectral accelerations for the hard rock site conditions. These maps have been prepared for five natural periods and four return periods by estimating hazard at the sites located at the nodes of a $0.2^\circ \times 0.2^\circ$ rectangular grid covering the entire region. A comprehensive study of the seismotectonic features and their relation with the past seismicity has been carried out to identify the potential seismic sources within 300 km around the region, and a total of 16 area-type sources of shallow crustal earthquakes and one dipping-plane source in the Hindukush

subduction zone have been identified. By using a comprehensive catalogue containing a total of 18,339 main shocks with magnitudes 3.5 or more for the period of 1501–2011, seismicity models with upper bound magnitudes have been developed to predict the occurrence rates of future earthquakes in each source. The seismicity in each source has been then distributed non-uniformly over the entire source zone area, based on the patterns of spatially smoothed epicentral density of past events, for estimating the occurrence rates of the earthquakes of different magnitudes in the source at various distances from a given site in the region.

In order to predict the ground motions at a given site due to the earthquakes in the 17 sources, two sets of published GMPEs have been shortlisted for the shallow crustal and subduction zone earthquakes, respectively. The candidate equations in each set have been then rated in terms of how closely those predict spectral accelerations for the limited set of ground motion records available in the region. Based on this analysis, the GMPEs by Abrahamson and Silva [72] and Lin and Lee [91] have been found to be most suitable for the shallow crustal and subduction zone earthquakes, respectively.

A comparison of the results obtained in this study with the provisions of the BIS code (BIS [1]) has raised the need for the upgradation of some of the Zone-IV regions in the code to Zone-V regions and the inclusion of Zone-VI in the code for the areas with PGA estimates significantly greater than $0.36\,g$. An improved expression has also been proposed for the standard spectral shape specified for Type I (rock or hard soil) in the code, which uses the MCE-level hazard estimates for PGA and 0.2-s period spectral acceleration. This will require the provision of an additional zoning map (for 0.2-s period spectral acceleration) besides the upgradation of the present zoning map for PGA. For a more detailed and site-specific design spectrum, the hazard maps prepared in this study for five natural periods may be used.

A hybrid approach has also been proposed based on the site response term in the GMPE by Abrahamson and Silva [72] to extend the hazard results obtained for the hard rock conditions to other soil conditions (with V_{S30} less than 1500 m/s). In this approach, the site amplification factor corresponding to the site response term of Abrahamson and Silva [72] is multiplied with a period-dependent modification factor defined empirically in terms of V_{S30} only.

This study has not considered the role of epistemic uncertainties and temporal variations in the occurrence rates of very large magnitude earthquakes. As regards temporal variations, the time-dependent seismicity models for large earthquakes predict significantly low occurrence rates for the small exposure periods of interest in engineering applications, thus leading to lower hazard levels than those obtained from the long-term average rates. This implies that the time-dependent models may not be able to introduce sufficient conservatism in the hazard results. Also, the available data are generally not sufficient to define the parameters of such models reliably. As regards epistemic uncertainties, those have been modeled arbitrarily in the past studies without sufficient justification or expert elicitation. In that respect, the use of the best choices for seismicity models and GMPEs (based on the available data and information), as in the present study, may be considered more appropriate than averaging the results of multiple choices without much scientific rationale. Moreover, higher conservatism on account of the epistemic uncertainties beyond that guaranteed by the results of the basic PSHA with best choices of various inputs and sufficiently long return periods may not be required for most engineering applications.

REFERENCES

1. BIS (2016). "IS 1893 (Part 1)—Criteria for Earthquake Resistant Design of Structures: Part 1 General Provisions and Buildings (Sixth Revision)", *Indian Standard, Bureau of Indian Standards, New Delhi*.
2. Basu, S. and Nigam, N.C. (1977). "Seismic Risk Analysis of Indian Peninsula", *Proceedings of the Sixth World Conference on Earthquake Engineering, New Delhi, India, Vol. I, pp. 782–790.*
3. Khattri, K.N., Rogers, A.M., Perkins, D.M. and Algermissen, S.T. (1984). "A Seismic Hazard Map of India and Adjacent Areas", *Tectonophysics, Vol. 108, No. 1-2, pp. 93–134*.
4. Bhatia, S.C., Ravi Kumar, M. and Gupta, H.K. (1999). "A Probabilistic Seismic Hazard Map of India and Adjoining Regions", *Annali di Geofisica, Vol. 42, No. 6, pp. 1153–1164*.

5. Parvez, I.A., Vaccari, F. and Panza, G.F. (2003). "A Deterministic Seismic Hazard Map of India and Adjacent Areas", *Geophysical Journal International, Vol. 155, No. 2, pp. 489–508*.
6. Costa, G., Panza, G.F., Suhadolc, P. and Vaccari, F. (1993). "Zoning of the Italian Territory in Terms of Expected Peak Ground Acceleration Derived from Complete Synthetic Seismograms", *Journal of Applied Geophysics, Vol. 30, No. 1-2, pp. 149–160*.
7. Boore, D.M. (2009). "Comparing Stochastic Point-Source and Finite-Source Ground-Motion Simulations: SMSIM and EXSIM", *Bulletin of the Seismological Society of America, Vol. 99, No. 6, pp. 3202–3216*.
8. Nath, S.K. and Thingbaijam, K.K.S. (2012). "Probabilistic Seismic Hazard Assessment of India", *Seismological Research Letters, Vol. 83, No. 1, pp. 135–149*.
9. Patil, N.S., Das, J., Kumar, A., Rout, M.M. and Das, R. (2014). "Probabilistic Seismic Hazard Assessment of Himachal Pradesh and Adjoining Regions", *Journal of Earth System Science, Vol. 123, No. 1, pp. 49–62*.
10. Boore, D.M. and Atkinson, G.M. (2008). "Ground-Motion Prediction Equations for the Average Horizontal Component of PGA, PGV, and 5%-Damped PSA at Spectral Periods between 0.01 s and 10.0 s", *Earthquake Spectra, Vol. 24, No. 1, pp. 99–138*.
11. Rout, M.M., Das, J., Das, K., Kamal and Das, R. (2015). "Probabilistic Seismic Hazard Assessment of NW and Central Himalayas and the Adjoining Region", *Journal of Earth System Science, Vol. 124, No. 3, pp. 577–586*.
12. Cornell, C.A. (1968). "Engineering Seismic Risk Analysis", *Bulletin of the Seismological Society of America, Vol. 58, No. 5, pp. 1583–1606.*
13. Cornell, C.A. (1971). "Probabilistic Analysis of Damage to Structures under Seismic Loads (in 'Dynamic Waves in Civil Engineering' Edited by D.A. Howells, I.P. Haigh, and C. Taylor)", *John Wiley & Sons, New York, U.S.A., pp. 473–488*.
14. McGuire, R.K. (1977). "Seismic Design Spectra and Mapping Procedures Using Hazard Analysis Based Directly on Oscillator Response", *Earthquake Engineering & Structural Dynamics, Vol. 5, No. 3, pp. 211–234*.
15. Richter, C.F. (1958). "Elementary Seismology", *W.H. Freeman, San Francisco, U.S.A.*
16. Molnar, P. and Tapponnier, P. (1975). "Cenozoic Tectonics of Asia: Effects of a Continental Collision", *Science, Vol. 189, No. 4201, pp. 419–426*.
17. GSI (2000). "Seismotectonic Atlas of India and Its Environs", *Technical Report, Geological Survey of India, Calcutta*.
18. Hodges, K.V. (2000). "Tectonics of the Himalaya and Southern Tibet from Two Perspectives", *The Geological Society of America Bulletin, Vol. 112, No. 3, pp. 324–350*.
19. Taylor, M., Yin, A., Ryerson, F.J., Kapp, P. and Ding, L. (2003). "Conjugate Strike-Slip Faulting along the Bangong-Nujiang Suture Zone Accommodates Coeval East-West Extension and North-South Shortening in the Interior of the Tibetan Plateau", *Tectonics, Vol. 22, No. 4, p. 1044*.
20. Singh, V.P., Duda, J. and Shanker, D. (2005). "A Plausible Model for the Present Day Seismicity and Tectonic Activity in the Hindukush Complex Zone", *Journal of Asian Earth Sciences, Vol. 25, No. 1, pp. 147–156.*
21. PMD-NORSAR (2007). "Seismic Hazard Analysis and Zonation for Pakistan, Azad Jammu and Kashmir", *Technical Report, Pakistan Meteorological Department, Islamabad, Pakistan and NORSAR, Kjeller, Norway*.
22. Robinson, A.C. (2009). "Geologic Offsets across the Northern Karakorum Fault: Implications for Its Role and Terrane Correlations in the Western Himalayan-Tibetan Orogen", *Earth and Planetary Science Letters, Vol. 279, No. 1-2, pp. 123–130*.
23. Taylor, M. and Yin, A. (2009). "Active Structures of the Himalayan-Tibetan Orogen and Their Relationships to Earthquake Distribution, Contemporary Strain Field, and Cenozoic Volcanism", *Geosphere, Vol. 5, No. 3, pp. 199–214*.
24. Lin, C., Yang, H., Liu, J., Rui, Z., Cai, Z. and Zhu, Y. (2012). "Distribution and Erosion of the Paleozoic Tectonic Unconformities in the Tarim Basin, Northwest China: Significance for the

Evolution of Paleo-Uplifts and Tectonic Geography during Deformation", *Journal of Asian Earth Sciences, Vol. 46, pp. 1–19*.

25. Seeber, L. and Armbruster, J.G. (1981). "Great Detachment Earthquakes along the Himalayan Arc and Long-Term Forecasting (in 'Earthquake Prediction: An International Review' Edited by D.W. Simpson and P.G. Richards)", *Technical Report, American Geophysical Union, Washington, D.C., U.S.A., pp. 259–277*.
26. Gupta, I.D. (2006). "Delineation of Probable Seismic Sources in India and Neighbourhood by a Comprehensive Analysis of Seismotectonic Characteristics of the Region", *Soil Dynamics and Earthquake Engineering, Vol. 26, No. 8, pp. 766–790*.
27. Searle, M., Hacker, B.R. and Bilham, R. (2001). "The Hindu Kush Seismic Zone as a Paradigm for the Creation of Ultrahigh-Pressure Diamond- and Coesite-Bearing Continental Rocks", *The Journal of Geology, Vol. 109, No. 2, pp. 143–153*.
28. Billington, S., Isacks, B.L. and Barazangi, M. (1977). "Spatial Distribution and Focal Mechanisms of Mantle Earthquakes in the Hindu Kush-Pamir Region: A Contorted Benioff Zone", *Geology, Vol. 5, No. 11, pp. 699–704*.
29. Pegler, G. and Das, S. (1998). "An Enhanced Image of the Pamir-Hindu Kush Seismic Zone from Relocated Earthquake Hypocenters", *Geophysical Journal International, Vol. 134, No. 2, pp. 573–595*.
30. Li, H., Van der Woerd, J., Sun, Z., Si, J., Tapponnier, P., Pan, J., Liu, D. and Chevalier, M.-L. (2012). "Co-seismic and Cumulative Offsets of the Recent Earthquakes along the Karakax Left-Lateral Strike-Slip Fault in Western Tibet", *Gondwana Research, Vol. 21, No. 1, pp. 64–87*.
31. Gupta, I.D. and Trifunac, M.D. (2019). "Attenuation of Fourier Amplitude and Pseudo Relative Velocity Spectra due to Local Earthquakes in the National Capital Region of India", *Soil Dynamics and Earthquake Engineering, Vol. 116, pp. 593–611*.
32. Oldham, T. (1883). "A Catalogue of Indian Earthquakes from the Earliest Time to the End of A.D. 1869", *Memoirs of the Geological Survey of India, Vol. XIX, pp. 163–215*.
33. Milne, J. (1911). "A Catalogue of Destructive Earthquakes: A.D. 7 to A.D. 1899", *Portsmouth Meeting Report, British Association for the Advancement of Science, London, U.K.*
34. Lee, W.H.K., Wu, F.T. and Jacobsen, C. (1976). "A Catalog of Historical Earthquakes in China Compiled from Recent Chinese Publications", *Bulletin of the Seismological Society of America, Vol. 66, No. 6, pp. 2003–2016*.
35. Quittmeyer, R.C. and Jacob, K.H. (1979). "Historical and Modern Seismicity of Pakistan, Afghanistan, Northwestern India, and Southeastern Iran", *Bulletin of the Seismological Society of America, Vol. 69, No. 3, pp. 773–823*.
36. Gutenberg, B. and Richter, C.F. (1954). "Seismicity of the Earth and Associated Phenomena", *Princeton University Press, Princeton, U.S.A.*
37. Gutenberg, B. (1956). "Great Earthquakes 1896-1903", *EOS, Transactions of American Geophysical Union, Vol. 37, No. 5, pp. 608–614.*
38. Rothé, J.P. (1969). "The Seismicity of the Earth, 1953–1965", *Technical Report, United Nations Educational, Scientific and Cultural Organization, Paris, France.*
39. Abe, K. (1994). "Instrumental Magnitudes of Historical Earthquakes, 1892 to 1898", *Bulletin of the Seismological Society of America, Vol. 84, No. 2, pp. 415–425*.
40. Abe, K. and Noguchi, S. (1983). "Determination of Magnitude for Large Shallow Earthquakes, 1898-1917", *Physics of the Earth and Planetary Interiors, Vol. 32, No. 1, pp. 45–59*.
41. Abe, K. and Noguchi, S. (1983). "Revision of Magnitudes of Large Shallow Earthquakes, 1897-1912", *Physics of the Earth and Planetary Interiors, Vol. 33, No. 1, pp. 1–11*.
42. Pacheco, J.F. and Sykes, L.R. (1992). "Seismic Moment Catalog of Large Shallow Earthquakes, 1900 to 1989", *Bulletin of the Seismological Society of America, Vol. 82, No. 3, pp. 1306–1349*.

43. Engdahl, E.R. and Villaseñor, A. (2002). "Global Seismicity: 1900-1999 (in 'International Handbook of Earthquake & Engineering Seismology, Part A' Edited by W.H.K. Lee, H. Kanamori, P.C. Jennings and C. Kisslinger)", *Academic Press, London, U.K., pp. 665–690*.
44. Ambraseys, N. (2000). "Reappraisal of North-Indian Earthquakes at the Turn of the 20th Century", *Current Science, Vol. 79, No. 9, pp. 1237–1250*.
45. Ambraseys, N.N. and Douglas, J. (2004). "Magnitude Calibration of North Indian Earthquakes", *Geophysical Journal International, Vol. 159, No. 1, pp. 165–206*.
46. Szeliga, W., Hough, S., Martin, S. and Bilham, R. (2010). "Intensity, Magnitude, Location, and Attenuation in India for Felt Earthquakes since 1762", *Bulletin of the Seismological Society of America, Vol. 100, No. 2, pp. 570–584*.
47. Raghukanth, S.T.G. (2010). "Catalogue of Earthquakes of Moment Magnitude ≥ 4.0 in and around India Assembled from Eighteen Sources (38860 Events Including Foreshocks and Aftershocks) (in 'Development of Probabilistic Seismic Hazard Map of India')", *Technical Report, The National Disaster Management Authority, New Delhi*.
48. Gutenberg, B. and Richter, C.F. (1956). "Magnitude and Energy of Earthquakes", *Annali di Geofisica, Vol. IX, No. 1, pp. 1–15*.
49. Chung, D.H. and Bernreuter, D.L. (1981). "Regional Relationships among Earthquake Magnitude Scales", *Reviews of Geophysics and Space Physics, Vol. 19, No. 4, pp. 649–663*.
50. Scordilis, E.M. (2006). "Empirical Global Relations Converting M_S and m_b to Moment Magnitude", *Journal of Seismology, Vol. 10, No. 2, pp. 225–236*.
51. Gardner, J.K. and Knopoff, L. (1974). "Is the Sequence of Earthquakes in Southern California, with Aftershocks Removed, Poissonian?", *Bulletin of the Seismological Society of America, Vol. 64, No. 5, pp. 1363–1367*.
52. Uhrhammer, R.A. (1986). Characteristics of Northern and Central California Seismicity, *Earthquake Notes, Vol. 57, No. 1, p. 21*.
53. Avouac, J.P., Tapponnier, P., Bai, M., You, H. and Wang, G. (1993). "Active Thrusting and Folding along the Northern Tien Shan and Late Cenozoic Rotation of the Tarim Relative to Dzungaria and Kazakhstan", *Journal of Geophysical Research, Vol. 98, No. B4, pp. 6755–6804*.
54. Yang, Y. and Liu, M. (2002). "Cenozoic Deformation of the Tarim Plate and the Implications for Mountain Building in the Tibetan Plateau and the Tian Shan", *Tectonics, Vol. 21, No. 6, pp. 9-1–9-17.*
55. Weichert, D.H. (1980). "Estimation of Earthquake Recurrence Parameters for Unequal Observation Periods for Different Magnitudes", *Bulletin of the Seismological Society of America, Vol. 70, No. 4, pp. 1337–1346*.
56. Stepp, J.C. (1972). "Analysis of Completeness of the Earthquake Sample in the Puget Sound Area and Its Effect on Statistical Estimates of Earthquake Hazard", *Proceedings of the International Conference on Microzonation for Safer Construction Research and Application, Seattle, U.S.A., Vol. 2, pp. 897–910*.
57. Tinti, S. and Mulargia, F. (1985). "Completeness Analysis of a Seismic Catalog", *Annales Geophysicae, Vol. 3, No. 3, pp. 407–414*.
58. Woessner, J. and Wiemer, S. (2005). "Assessing the Quality of Earthquake Catalogues: Estimating the Magnitude of Completeness and Its Uncertainty", *Bulletin of the Seismological Society of America, Vol. 95, No. 2, pp. 684–698*.
59. Albarello, D., Camassi, R. and Rebez, A. (2001). "Detection of Space and Time Heterogeneity in the Completeness of a Seismic Catalog by a Statistical Approach: An Application to the Italian Area", *Bulletin of the Seismological Society of America, Vol. 91, No. 6, pp. 1694–1703*.
60. Rotondi, R. and Garavaglia, E. (2002). "Statistical Analysis of the Completeness of a Seismic Catalogue", *Natural Hazards, Vol. 25, No. 3, pp. 245–258*.
61. Hainzl, S., Scherbaum, F. and Beauval, C. (2006). "Estimating Background Activity Based on Interevent-Time Distribution", *Bulletin of the Seismological Society of America, Vol. 96, No. 1, pp. 313–320*.

62. Herak, D., Herak, M. and Tomljenović, B. (2009). "Seismicity and Earthquake Focal Mechanisms in North-Western Croatia", *Tectonophysics, Vol. 465, No. 1-4, pp. 212–220*.
63. Hakimhashemi, A.H. and Grunthal, G. (2012). "A Statistical Method for Estimating Catalog Completeness Applicable to Long-Term Nonstationary Seismicity Data", *Bulletin of the Seismological Society of America, Vol. 102, No. 6, pp. 2530–2546*.
64. Anderson, J.G. (1979). "Estimating the Seismicity from Geological Structure for Seismic-Risk Studies", *Bulletin of the Seismological Society of America, Vol. 69, No. 1, pp. 135–158*.
65. Page, R. (1968). "Aftershocks and Microaftershocks of the Great Alaska Earthquake of 1964", *Bulletin of the Seismological Society of America, Vol. 58, No. 3, pp. 1131–1168*.
66. Cornell, C.A. and Vanmarcke, E.H. (1969). "The Major Influences on Seismic Risk", *Proceedings of the Fourth World Conference on Earthquake Engineering, Santiago, Chile, Vol. I, pp. A-1/69–93.*
67. Bommer, J.J. and Crowley, H. (2017). "The Purpose and Definition of the Minimum Magnitude Limit in PSHA Calculations", *Seismological Research Letters, Vol. 88, No. 4, pp. 1097–1106.*
68. Wheeler, R.L. (2009). "Methods of Mmax Estimation East of the Rocky Mountains", *Open-File Report 2009-1018, United States Geological Survey, Reston, U.S.A.*
69. Kijko, A. and Singh, M. (2011). "Statistical Tools for Maximum Possible Earthquake Magnitude Estimation", *Acta Geophysica, Vol. 59, No. 4, pp. 674–700*.
70. Bommer, J.J., Douglas, J., Scherbaum, F., Cotton, F., Bungum, H. and Fäh, D. (2010). "On the Selection of Ground-Motion Prediction Equations for Seismic Hazard Analysis", *Seismological Research Letters, Vol. 81, No. 5, pp. 783–793*.
71. Scherbaum, F., Cotton, F. and Smit, P. (2004). "On the Use of Response Spectral-Reference Data for the Selection and Ranking of Ground-Motion Models for Seismic-Hazard Analysis in Regions of Moderate Seismicity: The Case of Rock Motion", *Bulletin of the Seismological Society of America, Vol. 94, No. 6, pp. 2164–2185*.
72. Abrahamson, N. and Silva, W. (2008). "Summary of the Abrahamson & Silva NGA Ground-Motion Relations", *Earthquake Spectra, Vol. 24, No. 1, pp. 67–97*.
73. Campbell, K.W. and Bozorgnia, Y. (2008). "NGA Ground Motion Model for the Geometric Mean Horizontal Component of PGA, PGV, PGD and 5% Damped Linear Elastic Response Spectra for Periods Ranging from 0.01 to 10 s", *Earthquake Spectra, Vol. 24, No. 1, pp. 139–171*.
74. Chiou, B.S.-J. and Youngs, R.R. (2008). "An NGA Model for the Average Horizontal Component of Peak Ground Motion and Response Spectra", *Earthquake Spectra, Vol. 24, No. 1, pp. 173–215*.
75. Lee, V.W. (1987). "Influence of Local Soil and Geologic Site Conditions on Pseudo Relative Velocity Spectrum Amplitudes of Recorded Strong Motion Accelerations", *Report CE 87-06, University of Southern California, Los Angeles, U.S.A.*
76. Sharma, M.L., Douglas, J., Bungum, H. and Kotadia, J. (2009). "Ground-Motion Prediction Equations Based on Data from the Himalayan and Zagros Regions", *Journal of Earthquake Engineering, Vol. 13, No. 8, pp. 1191–1210*.
77. Anbazhagan, P., Kumar, A. and Sitharam, T.G. (2013). "Ground Motion Prediction Equation Considering Combined Dataset of Recorded and Simulated Ground Motions", *Soil Dynamics and Earthquake Engineering, Vol. 53, pp. 92–108*.
78. Ramkrishnan, R., Kolathayar, S. and Sitharam, T.G. (2019). "Development of New Ground Motion Prediction Equation for the North and Central Himalayas Using Recorded Strong Motion Data", *Journal of Earthquake Engineering, DOI: 10.1080/13632469.2019.1605318*.
79. Gupta, I.D. and Trifunac, M.D. (2018). "Empirical Scaling Relations for Pseudo Relative Velocity Spectra in Western Himalaya and Northeastern India", *Soil Dynamics and Earthquake Engineering, Vol. 106, pp. 70–89*.
80. Gupta, I.D. and Trifunac, M.D. (2018). "Attenuation of Strong Earthquake Ground Motion—I: Dependence on Geology along the Wave Path from the Hindu Kush Subduction to Western Himalaya", *Soil Dynamics and Earthquake Engineering, Vol. 114, pp. 127–146.*

81. Gupta, I.D. (2013). "Source-to-Site Distance Distributions for Area Type of Seismic Sources Used in PSHA Applications", *Natural Hazards, Vol. 66, No. 2, pp. 485–499*.
82. Leonard, M. (2010). "Earthquake Fault Scaling: Self-Consistent Relating of Rupture Length, Width, Average Displacement, and Moment Release", *Bulletin of the Seismological Society of America, Vol. 100, No. 5A, pp. 1971–1988*.
83. Campbell, K.W. and Bozorgnia, Y. (2007). "Campbell-Bozorgnia NGA Ground Motion Relations for the Geometric Mean Horizontal Component of Peak and Spectral Ground Motion Parameters", *Report PEER 2007/02, Pacific Earthquake Engineering Research Center, University of California, Berkeley, U.S.A.*
84. Gupta, I.D. (2018). "Uniformly Processed Strong Motion Database for Himalaya and Northeast Region of India", *Pure and Applied Geophysics, Vol. 175, No. 3, pp. 829–863*.
85. Jaisal, A.K. (2016). "A Comprehensive Probabilistic Seismic Hazard Mapping of Northwest Indian States Using PSHA Approach", *M.Tech. Thesis, Department of Civil Engineering, Indian Institute of Technology Kanpur, Kanpur*.
86. Mittal, H., Kumar, A. and Ramhmachhuani, R. (2012). "Indian National Strong Motion Instrumentation Network and Site Characterization of Its Stations", *International Journal of Geosciences, Vol. 3, No. 6A, pp. 1151–1167*.
87. Abrahamson, N.A. and Somerville, P.G. (1996). "Effects of the Hanging Wall and Footwall on Ground Motions Recorded during the Northridge Earthquake", *Bulletin of the Seismological Society of America, Vol. 86, No. 1B, pp. S93–S99*.
88. Somerville, P. and Pitarka, A. (2006). "Differences in Earthquake Source and Ground Motion Characteristics between Surface and Buried Faulting Earthquakes", *Proceedings of the Eighth U.S. National Conference on Earthquake Engineering, San Francisco, U.S.A., Paper No. 977 (on CD)*.
89. Atkinson, G.M. and Boore, D.M. (2003). "Empirical Ground-Motion Relations for Subduction-Zone Earthquakes and Their Application to Cascadia and Other Regions", *Bulletin of the Seismological Society of America, Vol. 93, No. 4, pp. 1703–1729*.
90. Gupta, I.D. (2010). "Response Spectral Attenuation Relations for In-Slab Earthquakes in Indo-Burmese Subduction Zone", *Soil Dynamics and Earthquake Engineering, Vol. 30, No. 5, pp. 368–377*.
91. Lin, P.-S. and Lee, C.-T. (2008). "Ground-Motion Attenuation Relationships for Subduction-Zone Earthquakes in Northeastern Taiwan", *Bulletin of the Seismological Society of America, Vol. 98, No. 1, pp. 220–240*.
92. Youngs, R.R., Chiou, S.-J., Silva, W.J. and Humphrey, J.R. (1997). "Strong Ground Motion Attenuation Relationships for Subduction Zone Earthquakes", *Seismological Research Letters, Vol. 68, No. 1, pp. 58–73*.
93. Zhao, J.X., Zhang, J., Asano, A., Ohno, Y., Oouchi, T., Takahashi, T., Ogawa, H., Irikura, K., Thio, H.K., Somerville, P.G., Fukushima, Y. and Fukushima, Y. (2006). "Attenuation Relations of Strong Ground Motion in Japan Using Site Classification Based on Predominant Period", *Bulletin of the Seismological Society of America, Vol. 96, No. 3, pp. 898–913*.
94. Anderson, J.G. and Trifunac, M.D. (1978). "Uniform Risk Functionals for Characterization of Strong Earthquake Ground Motion", *Bulletin of the Seismological Society of America, Vol. 68, No. 1, pp. 205–218*.
95. Gupta, I.D. (2009). "Seismic Hazard Mapping Methodologies", *Proceedings of the International Conference on Earthquake Engineering—On the Occasion of the 40th Anniversary of Banja Luka Earthquake", Banja Luka, Bosnia & Herzegovina, pp. 55–101*.
96. Petersen, M.D., Frankel, A.D., Harmsen, S.C., Mueller, C.S., Haller, K.M., Wheeler, R.L., Wesson, R.L., Zeng, Y., Boyd, O.S., Perkins, D.M., Luco, N., Field, E.H., Wills, C.J. and Rukstales, K.S. (2008). "Documentation for the 2008 Update of the United States National Seismic Hazard Maps", *Open-File Report 2008-1128, United States Geological Survey, Menlo Park, U.S.A.*
97. Kaklamanos, J., Baise, L.G. and Boore, D.M. (2011). "Estimating Unknown Input Parameters When Implementing the NGA Ground-Motion Prediction Equations in Engineering Practice", *Earthquake Spectra, Vol. 27, No. 4, pp. 1219–1235*.

98. Pagani, M., Monelli, D., Weatherill, G., Danciu, L., Crowley, H., Silva, V., Henshaw, P., Butler, L., Nastasi, M., Panzeri, L., Simionato, M. and Vigano, D. (2014). "OpenQuake-Engine: An Open Hazard (and Risk) Software for the Global Earthquake Model", *Seismological Research Letters, Vol. 85, No. 3, pp. 692–702*.
99. Campbell, K.W. and Gupta, N. (2018). "Modeling Diffuse Seismicity in Probabilistic Seismic Hazard Analysis: Treatment of Virtual Faults", *Earthquake Spectra, Vol. 34, No. 3, pp. 1135–1154*.
100. ICC (2006). "2006 International Building Code", *International Code Council, Inc., Country Club Hills, U.S.A.*
101. ASCE (2010). "ASCE/SEI 7-10: Minimum Design Loads for Buildings and Other Structures", *ASCE Standard, American Society of Civil Engineers, Reston, U.S.A.*
102. Kanagarathinam, L., Dodagoudar, G.R. and Boominathan, A. (2008). "Probabilistic Seismic Hazard Studies of East Coast Region of India", *Proceedings of the 14th World Conference on Earthquake Engineering, Beijing, China (on CD)*.
103. Revathi, P. and Pandurangan, K. (2012). "Seismic Hazard Analysis of Puducherry Region", *International Journal of Earth Sciences and Engineering, Vol. 5, No. 2, pp. 219–223*.
104. Sitharam, T.G. and Kolathayar, S. (2013). "Seismic Hazard Analysis of India Using Areal Sources", *Journal of Asian Earth Sciences, Vol. 62, pp. 647–653*.
105. NDMA (2010). "Development of Probabilistic Seismic Hazard Map of India", *Technical Report, The National Disaster Management Authority, New Delhi*.
106. Algermissen, S.T. and Perkins, D.M. (1976). "A Probabilistic Estimate of Maximum Acceleration in Rock in the Contiguous United States", *Open-File Report 76-416, United States Geological Survey, Menlo Park, U.S.A.*
107. Joyner, W.B. and Boore, D.M. (1981). "Peak Horizontal Acceleration and Velocity from Strong-Motion Records Including Records from the 1979 Imperial Valley, California, Earthquake", *Bulletin of the Seismological Society of America, Vol. 71, No. 6, pp. 2011–2038*.
108. Goulet, C.A. and Stewart, J.P. (2009). "Pitfalls of Deterministic Application of Nonlinear Site Factors in Probabilistic Assessment of Ground Motions", *Earthquake Spectra, Vol. 25, No. 3, pp. 541–555*.